Water Resources Research

RESEARCH ARTICLE
10.1029/2024WR038364

A Novel Surface-Based Approach to Represent Aquifer Heterogeneity in Sedimentary Formations

Ludovic Schorpp[1], **Julien Straubhaar**[1], **and Philippe Renard**[1]

[1]Center for Hydrogeology and Geothermics, University of Neuchâtel, Neuchâtel, Switzerland

Key Points:

- A new surface-based stochastic facies modeling algorithm is presented
- It is flexible and relies on few parameters to produce a variety of geological settings
- The proposed method can efficiently reproduce observed fluvio-glacial structures

Correspondence to:

L. Schorpp,
ludovic.schorpp@unine.ch

Citation:

Schorpp, L., Straubhaar, J., & Renard, P. (2025). A novel surface-based approach to represent aquifer heterogeneity in sedimentary formations. *Water Resources Research*, *61*, e2024WR038364. https://doi.org/10.1029/2024WR038364

Received 11 JUL 2024
Accepted 9 JAN 2025

Author Contributions:

Conceptualization: Philippe Renard
Methodology: Julien Straubhaar, Philippe Renard
Supervision: Philippe Renard
Validation: Julien Straubhaar
Writing – review & editing: Julien Straubhaar, Philippe Renard

Abstract Sedimentary formations that compose most aquifers are difficult to model as a result of the nature of their deposition. Their formation generally involves multiple processes (alluvial, glacial, lacustrine, etc.) that contribute to the complex organization of these deposits. Representative models can be obtained using process-based or rule-based methods. However, such methods have several drawbacks: complicated parameterization, large computing time, and challenging, if not impossible, conditioning. To address these problems, we propose a new simple hierarchical surface-based algorithm, named EROSim. First, a predefined number of stochastic surfaces are simulated in a given order (from older to younger). These surfaces are simulated independently but interact with each other through erosion rules. Each surface is either an erosive or a deposition surface. The deposition surfaces represent the boundaries of depositional events, whereas the erosive surfaces can remove parts of the previously simulated deposits. Finally, these surfaces delimit sedimentary regions that are filled with facies. The approach is quite simple, general, flexible, and can be conditioned to borehole data. The applicability of the method is illustrated using data from fluvio-glacial sedimentary deposits observed in the Bümberg quarry in Switzerland.

1. Introduction

Groundwater flow and solute transport processes including dispersion, mixing, or chemical reactions are heavily influenced by geological heterogeneity occurring at multiple scales (Bennett et al., 2017; Chiogna et al., 2015; Kitanidis, 2015; Soltanian et al., 2020; Wallace et al., 2021). To investigate the impact of geological heterogeneity on these processes, multiGaussian random functions are often used (Chiles & Delfiner, 2012; Dagan, 1989; Geng et al., 2020; Rubin, 2003; Zech et al., 2021) because they provide a parsimonious but flexible mathematical framework. To incorporate more geological concepts and knowledge in these analyses and to account for different types of connectivity, alternative models (from process-based to structure-imitating approaches) have also been developed for a wide range of geological environments (de Marsily et al., 2005; Koltermann & Gorelick, 1996).

In this paper, we propose a new simple model to represent the geological heterogeneity produced by sedimentary processes in unconsolidated fluvio-glacial environments. We focus on this geological setting because it contains the most heavily exploited groundwater resources in Switzerland (and many other countries) for drinking water supply and shallow geothermal energy use. Being close to the surface, these aquifers are also prone to anthropogenic contamination, and therefore, describing their internal heterogeneity is important for the analysis of contaminant transport.

These formations are the result of a rich and complex sedimentological history (Miall, 1996). Outcrop observations and geostatistical analysis show that fluvio-glacial sediments are structured in a hierarchical manner (Bayer et al., 2011; Heinz et al., 2003; Miall, 1996; Ritzi et al., 2004). Therefore modeling approaches aiming at studying the impact of this type of heterogeneity should also include these hierarchical relationships. One way to achieve this aim is to construct directly a hierarchical multiGaussian model (Neuman et al., 2008). To integrate more geological concepts, Scheibe and Freyberg (1995) and Ramanathan et al. (2010), used sophisticated object-based methods where sedimentary structures are created hierarchically following sedimentological rules. Webb (1994) or Pirot et al. (2015) proposed also a hierarchical approach, where multiple geomorphological surfaces are stochastically generated and stacked together to define the major units. These units are then filled with facies using a deformation process (Pirot et al., 2015) or based on an estimation of the Froude number (Webb, 1994). While these methods provide models that exhibit realistic geological features, they are difficult to constrain to field data and borehole observations. Comunian et al. (2011) or Bennett et al. (2019) decompose the problem and model a set of surfaces that delimit volumes that can then be filled with other facies simulation techniques. Zuffetti et al. (2020) describe in detail the limitations of the methods that do not account for the

stratigraphical hierarchy. Following these observations, Zuffetti et al. (2020) introduced a generic framework to overcome these limitations by defining how sub-units should be modeled into larger units at multiple scales. Based on these concepts, Schorpp et al. (2022) proposed the ArchPy approach that is capable of handling the hierarchical relations when constructing a 3D geological model. This approach has been coupled with geophysical and hydrogeological inversion and applied successfully to synthetic data (Neven, Schorpp, & Renard, 2022) and to characterize the northern area of the upper Aare fluvio-glacial aquifer in Switzerland (Neven & Renard, 2023). ArchPy is also a python library for geological modeling that can integrate various geostatistical methods such as Multiple Point Statistics (Strebelle, 2002). In this context, the development and integration of new facies modeling methods is sought.

In this paper, we propose to go a step further and develop the EROSim method that allows filling the stratigraphic units with detailed facies models while ensuring conditioning. The proposed method belongs to the family of surface-based methods (SBM) that emerged in the early 2000s (Pyrcz & Deutsch, 2014) with the pioneering work of Xie et al. (1999, 2001). SBMs consider that the different geological features (layers, architectural elements, facies, etc.) can be separated by surfaces (Jo et al., 2020; Pyrcz et al., 2015; Titus et al., 2021). These methods also integrate the notion of time during which geological objects are deposited. The different surfaces are stacked on top of each other and delimit the geological units or sediment types. The surfaces can either be deterministic or stochastic. Compared to pixel-based methods, SBM can maintain complex geometries such as independent regions throughout the modeling process, which is an advantage when it comes to accounting for the internal heterogeneity of these different regions.

The general idea of the proposed approach consists of generating multiple stochastic surfaces and combining them to delimit the different rock types or lithofacies. This strategy is highly flexible and allows performing conditional simulations even with a complex and realistic sedimentary structure. One important aspect of the proposed model is that we aimed to keep the model parameterization as simple as possible to facilitate its practical applications. This goes against most of the previous works which provide much more detailed representations of a broad diversity of sedimentary architectural elements, but on the counterpart, these previous models require a more complex parameterization and are more difficult to condition to actual borehole observations. Our modeling decisions involve limitations in the sedimentological interpretation of the resulting facies model but the proposed model is easier to apply.

We show in the paper how this model is capable of simulating and extending detailed sedimentary structures that are directly observable in outcrops. We also show that this model can be used to represent heterogeneity at the decametric to hectometric scale in aquifers and estimate their flow and transport properties more accurately than the frequently used SIS method.

The paper is organized as follows. We first introduce the proposed simulation methodology in Section 2. Section 3 illustrates the sensitivity of the method to its parameters and shows how it compares to other facies simulation techniques in simple cases. Then, in Section 4, we illustrate how this model can be used to represent and extend detailed information collected on outcrops in a gravel pit in the upper Aare Valley in Switzerland. In addition, flow and advection transport modeling is carried out to further validate the use of our methodology The relevance of the results and the different advantages and limitations of the method are discussed in Section 5.

2. A Surface-Based Approach to Represent Aquifer Heterogeneity

This section describes the EROSim approach and its implementation. First, the general workflow is introduced, we then present the notations and definitions that are used in the following to describe precisely each step of the method.

2.1. General Principle

The principle of the method is to decompose the simulation domain into multiple regions (or volumes) using stochastic surfaces. Each region for each simulation corresponds to a single categorical value representing a lithology, a facies, or a unit, in a finite 2D or 3D domain. The three main steps of the method are therefore the following.

1. *Surface simulation.* A set of surfaces are stochastically simulated and modified according to erosion rules. These surfaces can either be depositional or erosional.

2. *Region delimitation*. The ensemble of surfaces simulated in step 1 forms a tessellation of the simulation domain, where each tile is individualized as a region. A graph of the spatial relationships between the regions is constructed.
3. *Facies assignment*. During this step, a facies is assigned to each of the regions defined in step 2 while accounting for the spatial continuity of the facies.

2.2. Notations and Definitions

The simulation domain is denoted $\Omega \subset \mathbb{R}^n$ where $n = 2$ or 3 is its spatial dimension. We then consider a finite set of lithofacies $\mathbf{K} = \{K_1, K_2, \dots, K_k\}$, where k is the number of facies to simulate. The goal is to obtain a stochastic process f that can map any location to a certain facies such that $f : \Omega \rightarrow \mathbf{K}$.

We also consider a number of ordered stochastic surfaces S_t that delimit different regions V_i stored in a set $\mathbf{V}$. Each volume can only take one value in $\mathbf{K}$, that is, f is constant on each volume V_i. The subscript $t \in \mathbb{N}$ in S_t represents the simulation time step and can be seen as analogous to geological time. These surfaces are stochastic processes of dimension $n - 1$, which means, for example, that if the simulation domain is in 3D ($n = 3$), S_t are 2D stochastic surfaces. The regions V_i are objects of dimension n each corresponding to a single connected component, they do not intersect each other. Furthermore, the ensemble of all the V_i fills Ω. We can also refer to the V_i as areas if $n = 2$ or volumes if $n = 3$. The boundaries S_t are ordered by age (from younger to older) in a list $\mathbf{S}$. The order of the surfaces is important because it represents the sedimentological history of the simulation domain and has consequences on the interactions that can exist between the surfaces through erosion rules.

An important aspect of stochastic geological models is their ability to be conditioned by borehole data. In this study, each borehole is assumed to be 1D and vertical. The list of boreholes is denoted $\mathbf{B}$. A borehole contains a sequence of contiguous intervals. For a simulation in 2D (resp. 3D), a borehole is located by a position $\mathbf{x} = (x)$ (resp. $\mathbf{x} = (x, y)$). The facies encountered along the borehole are defined with a sequence of elevations $z_1 < \dots < z_m$ and a sequence of facies $k_1, \dots k_{m-1} \in \mathbf{K}$. The i-th interval between the bottom and top elevations z_i and z_{i+1}, is filled with the facies k_i, that is, $f(\mathbf{x}, z) = k_i$ if $z_i \leq z < z_{i+1}$ (and $(\mathbf{x}, z) \in \Omega$), for $i = 1, \dots, m$. Hence, a borehole B is expressed as $B = (\mathbf{x}, \{z_1, \dots, z_m\}, \{k_1, \dots, k_{m-1}\})$ or as $B = (\mathbf{x}, ([z_1, z_2[, k_1), \dots, ([z_{m-1}, z_m[, k_{m-1}))$.

2.3. Unconditional Simulation

The unconditional simulation algorithm is summarized in Algorithm 1. The steps are described in detail below.

Algorithm 1. Unconditional Algorithm

Require: Parameters
N: integer - number of simulated depositional surfaces
$\gamma_0, \dots, \gamma_{N-1}$: covariance (or variogram) models for each surface
$\mu_0, \dots, \mu_{N-1}$: mean elevations for each surface
ξ: in $[0, 1]$ - proportion of eroding surfaces
p_{global}: target proportions of the facies, over the whole domain
α: in $[0, 1]$ - clustering parameter

1: Order all the surfaces in $\mathbf{S}$ by their means (μ_i) ▷ see Section 2.3.1
2: Set surface index $t = 0$
3: **while** $t < N$ **do** ▷ see Section 2.3.2
4: Determine if S_t is erode or onlap, given ξ
5: Unconditional simulation
6: **if** S_t is *onlap* **then**
7: $t = t + 1$
8: Apply erosion-deposition Rules (EDR, Equations 3 and 4)
9: Define regions V_i ▷ see Section 2.3.3
10: Assign facies to V_i using Algorithm 2 (depending on p_{global}, α)

2.3.1. Surface Ordering

Assuming that the parameters are defined, and before generating the surfaces, the first step (line 1) consists of checking the input parameters and ordering the surfaces by their mean elevation (from low to high).

This sorting is used to represent the evolution of geological time, with each event (a surface) occurring one after the other. Proceeding that way, we assume that the geological processes gradually increase upward due to the gradual accumulation of the sediments in the system.

2.3.2. Surface Simulation

The second step consists of simulating N depositional surfaces through the domain Ω. Each time a new surface is simulated, from oldest to youngest, erosion-deposition rules (EDR) are applied. We consider here only the depositional surfaces because the erosion events are assumed to deposit no sediments, as explained below. Note that this part of the methodology does not seek to represent exactly the complex process of sediment deposition and erosion, but rather draws inspiration from it to create a tessellation of the domain.

Let S_t be the simulated surface at time t, before applying the EDR. In the following examples, S_t is modeled as a Gaussian Random Field (GRF) following a specified mean μ_t and a specified covariance (or variogram) model γ_t. But, the mathematical model used to simulate the surfaces could be different. We use GRFs for convenience and simplicity. GRFs are easy to simulate (Chiles & Delfiner, 2012) and to constrain (useful for the conditional case). They are also flexible as they can handle non-stationary mean or covariance parameters. To generate our GRFs, we used the Geone (http://www.github.com/randlab/geone) python library that provides a set of common geostatistical, Multiple Point Statistics modeling and image analysis tools.

In the following, for illustration purposes, we generally consider that all the surfaces follow the same covariance model (all γ_i are identical) but differ from each other by their mean. Moreover, the stochastic processes are assumed stationary, that is, the mean and covariance are constant spatially.

Every surface S_t can be expressed as a function $S_t = S_t(\mathbf{x})$, defined for spatial locations $\mathbf{x} \in \mathbb{R}^{n-1}$. Let us then denote by S_t^* the surface at time t modified by the application of the EDR.

At time $t = 0$, the surface S_0^* is initialized as

$$S_0^*(\mathbf{x}) \leftarrow S_0(\mathbf{x}). \tag{1}$$

For the following time steps ($t > 0$), we first determine if the event is an erosional event or a depositional event. The decision is randomized based on the probability ξ given by the user. This probability represents the fraction of erosive events among all the geological events (deposition and erosion) that are simulated. From a geological point of view, this parameter can be interpreted as the frequency of occurrence of an erosive event, which varies according to the geological setting. For example, this erosive event in alluvial and abyssal settings can be attributed to an avulsion (Allen, 1978; Bridge & Leeder, 1979; Pirmez et al., 2000), and in a glacial setting it is generally the result of major glacial advances or important glacial fluctuations (Solomina et al., 2015).

Then, we generate a new surface.

$$S_t = \mathrm{GRF}(\mu_t, \gamma_t). \tag{2}$$

If the event is depositional, we apply the depositional rule:

$$S_t^*(\mathbf{x}) \leftarrow \max(S_t(\mathbf{x}),\ S_{t-1}^*(\mathbf{x})). \tag{3}$$

and increment the value of t for the next iteration. For depositional events (Equation 3), if the simulated surface is below a part of a previously simulated surface, there is no deposition and the elevation at that location is equal to the latter.

Otherwise, if the event is erosive, the computed surface S_t erodes the previously deposited formations.

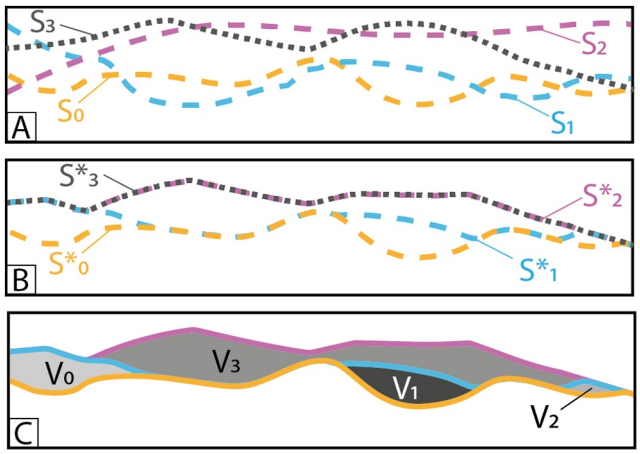

Figure 1. Schematic representation of the delimitation procedure for the regions. (a) four surfaces have been simulated: yellow, blue, pink, and gray. The last one (gray) is eroding while the others are onlap. (b) Situation after the application of the deposition and erosion rules. (c) distinct regions are differentiated.

$$S_k^*(\mathbf{x}) \leftarrow \min\left(S_t(\mathbf{x}),\ S_k^*(\mathbf{x})\right), \quad \text{for } k = 0, \dots, t-1 \tag{4}$$

All previously simulated surfaces that are above the simulated erosional surfaces are updated (Equation 4). The time t is not incremented in that situation.

A schematic representation of these rules is shown in Figures 1a and 1b. In this example, the first three surfaces are depositional and the last (S_3) is erosive. The surfaces S_0, S_1, and S_2 are first simulated and adjusted according to the first two equations (Equations 1 and 3), and the surface S_3 erodes them where S_3 is simulated below the others (Equation 4).

2.3.3. Region Delimitation

Once the surfaces have been simulated and the EDR applied (Algorithm 1, lines 1 to 10), the simulation domain Ω is divided into distinct regions. All of these regions V_i are defined by exactly two successive (in simulation time) onlap surfaces (two depositional events), one delimiting its top and the other its base. A region can only exist where its top surface is strictly above its bottom surface. It does not exist where the two surfaces are exactly at the same elevation. This implies that regions are delimited on the sides when the top and bottom surfaces meet. If multiple distinct regions occur between two surfaces, they will be treated as independent regions. This means that later in the simulation, different facies may be assigned to these regions, even if they are defined by the same surfaces. This is in contrast to previous studies, where each simulated surface delimits one sedimentological entity (Pirot et al., 2015; Pyrcz et al., 2005; Webb, 1994). This feature allows the simulation of different types of sediments in different locations during a sedimentological event as it is expected to occur when sediment sorting occurs. But, the method is based only on a statistical description and geometric reasoning. It does not rely on any sedimentological rule with the aim of keeping the parameterization very simple and parsimonious.

In practice, the individual regions are identified as the connected components of the sets $\left\{(\mathbf{x}, z) \in \Omega \ : \ S_t^*(\mathbf{x}) \leq z < S_{t+1}^*(\mathbf{x})\right\}$, $t = 0, \dots, N-1$, where N is the total number of onlap surfaces simulated. Finally, two supplementary regions, made up of all points of Ω respectively below the surface S_0^* and above the last surface S_{N-1}^*, are added, to cover the entire simulation domain. Alternatively, Ω can be reduced to the domain between S_0^* and S_{N-1}^*. An example of region delimitation in 2D is illustrated in Figure 1c.

2.3.4. Facies Attribution

The aim is to assign a facies to each of the regions V_i determined in the previous step. To do so, we propose a simple algorithm that is summarized in Algorithm 2.

Algorithm 2. Graph-Based Indicator Simulation

Require: Parameters
p_{global}: global proportions of the facies, over the whole domain
α: in $[0, 1]$ - clustering parameter
$\mathbf{V}$: set of regions covering the whole domain
G: a spatial graph G representing the connections of the regions

1: $V_i \leftarrow$ select a random region in $\mathbf{V}$
2: $p_{target} \leftarrow$ compute target proportions using Equation 6
3: if $\alpha < 1$ **then**
4: $\mathbf{V}_J \leftarrow$ get the neighbours of V_i using G
5: $p_{neig} \leftarrow$ compute the local proportions using Equation 7
6: else
7: $p_{neig} = 0$ (unused)

8: $p_{V_i} \leftarrow$ compute facies probabilities for V_i using Equation 8
9: Draw a facies in K according to p_{V_i} and assign it to V_i
10: Update the global current proportions p_{cur}
11: Go to 1 until all regions are filled

We are assuming that based on borehole or outcrop data, the user can provide an estimate of the target global facies proportions p_{global} in the study area, for example, 50% of sand, 20% of gravel, and 30% of clay. In addition, we want to provide a simple parameterization allowing the user to control the spatial continuity of the facies. For this, we introduce a clustering parameter α that the user can adjust.

The attribution then follows a simple method with adaptive target proportions to respect as well as possible the global facies proportions and spatial continuity. The idea is to sequentially populate the regions with random facies according to a probability distribution adapted for each region. At each step, a region is randomly selected to avoid any systematic bias in the final simulations, and the facies probabilities are updated. Before assigning the facies, the target facies probabilities are first computed accounting for the global target proportions p_{global}, the current proportions p_{cur} over the already simulated regions, and also the local proportions derived from the surrounding regions.

First, target proportions p_{target} are calculated such that

$$\phi p_{cur} + (1 - \phi) p_{target} = p_{global}, \tag{5}$$

where ϕ is the ratio of the total volume of the already simulated regions over the volume of Ω. Equation 5 means that if the entire non-simulated volume was filled with proportions p_{target}, the final proportion over Ω would be p_{global}. The target proportions are explicitly expressed as

$$p_{target} = \frac{p_{global} - \phi p_{cur}}{(1 - \phi)}. \tag{6}$$

If p_{target} for a certain facies becomes negative, it is set to 0 and the proportions for the other facies are rescaled so that the sum of p_{target} is equal to 1. This situation can occur when a current proportion is too high ($\phi p_{cur}(i)$ exceeds $p_{global}(i)$ for some component i). It is important to understand that p_{target} is computed before the facies attribution of each region, and then it can vary since it depends on p_{cur} and ϕ. Therefore, the global target proportions for the unsimulated part of the domain are continuously corrected until the simulation is finished.

Secondly, to introduce some spatial continuity, the local proportions p_{neigh} are computed from the regions around the simulated one. This is done by using a spatial graph G describing the regions and their contacts. Each vertex in G refers to a region, and an edge links two vertices if the two corresponding regions are in contact (adjacent). The size of the contact (length if $n = 2$ or area if $n = 3$) is the weight attached to the edge. An example in 2D is shown in Figures 2a and 2b. Note that the graph is constructed prior to the facies assignment procedure.

We consider V_i the region in which a facies has to be attributed (currently simulated region) and $\mathcal{J}$ the set of indices j of the regions adjacent to V_i, that is, $j \in \mathcal{J}$ when the vertices corresponding to V_i and V_j are linked in G by an edge, of weight w_{i-j}. These weights correspond to the length of contact between the region V_i and V_j to weight the neighborhood effect. This ensures that a neighbor that barely touches a region does not have as much weight as a region that is in close contact with it. Then, the local facies probabilities p_{neig} for V_i are defined based on the neighbors V_j as follows:

$$p_{neig} = \frac{\sum_{j \in \mathcal{J}} w_{i-j} \cdot p_{V_j}}{\sum_{j \in \mathcal{J}} w_{i-j}} \tag{7}$$

where p_{V_j} is the proportions of facies in the neighbor region V_j. The vector p_{V_j} is of length k where k is the number of facies and it is defined as follows. If a facies K_l has already been assigned in V_j, then all the components of p_{V_j}

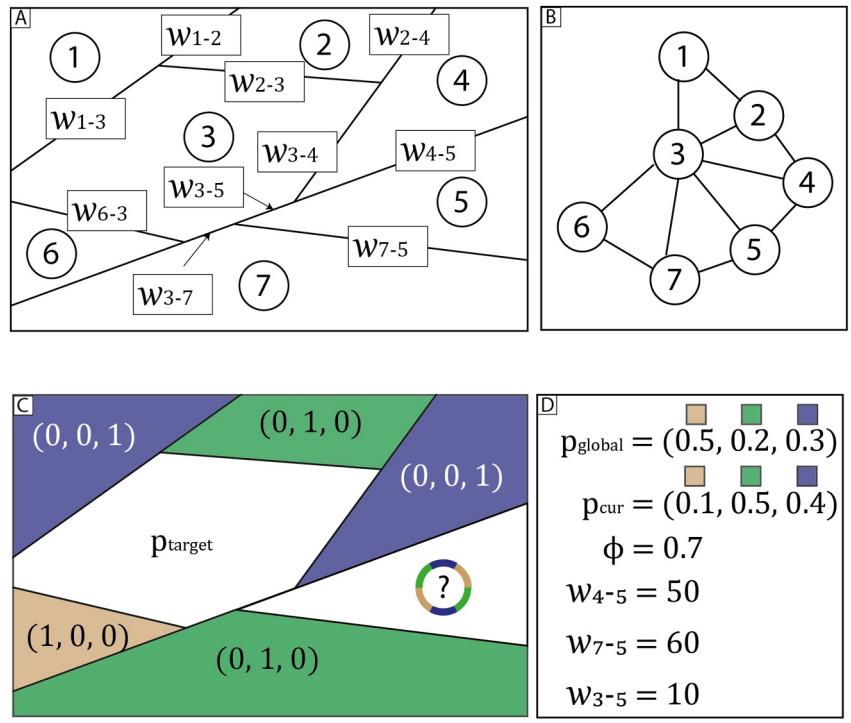

Figure 2. Conceptual representation of a 2D simulation domain separated in seven regions (a) and its associated spatial graph (b). The w_{i-j} correspond to the length of contact between V_i and V_j, they are used as weights for the edges in the graph. (c) represents a situation during the attribution of the facies (three in total) for volume 5. The facies proportions are written in each region (note that region 3 is not defined at this point of the simulation and the modified global proportion p_{target} is used). (d) details the variables required to compute the probability mass used to draw a facies in region 5 (see text for details).

are set to 0 except the l-th component that is set to 1. If V_j is a region not yet simulated (with no assigned facies), then p_{V_j} is set to the target proportions p_{target} computed above.

Finally, the probability distribution, p_{V_i}, used to draw a facies in the region V_i is obtained by combining probabilities p_{target} and p_{neigh} (see Equations 5 and 6) via a log-linear pooling operator (Allard et al., 2012):

$$p_{V_i} = (p_{target})^{\alpha}(p_{neig})^{1-\alpha} \tag{8}$$

where α is a user-defined parameter ranging from 0 to 1 that controls the clustering of the regions of identical facies. If $\alpha = 0$, the same facies are more likely to be adjacent and, in contrast, if $\alpha = 1$, the facies are drawn only according to p_{target} (p_{neigh} is ignored).

The main advantage of this method is that it is simple and requires only the global target proportion p_{global} and the parameter α as input. Note that the graph-based approach presented here is applied to a domain divided into tiles and then is independent of the first part of the EROSim methodology. More complex methods could be considered, such as those using rules to guide the position of the facies (e.g., by constraining some facies to appear more frequently in small regions).

To illustrate the procedure, let us consider the 2D case shown in Figure 2c, based on the domain delimitation in Figure 2a. Here the facies in V_5 have to be drawn from p_{V_5} using Equation 8. First, we need to calculate p_{target} which depends on p_{cur} and ϕ (Equation 6). We obtain $p_{target} = \left(\frac{43}{30}, -\frac{1}{2}, \frac{1}{15}\right)$ which after setting the second probability to 0 and rescaling becomes: $p_{target} = \left(\frac{43}{45}, 0, \frac{2}{45}\right) \approx (0.96, 0, 0.04)$. Then we need to compute p_{neig}, which depends on the facies in the regions surrounding V_5, which are V_3, V_4, V_7 according to the graph. Applying Equation 7 with values in Figure 2 gives: $p_{neig} = (0.08, 0.50, 0.42)$ which is very different from p_{target}. We see that the most probable facies according to neighbors are, in fact, the green and blue facies, as they share the longest

contact length with V_5. We can also note that since the facies proportion is undefined in region 3, p_{target} is taken for that region. Finally, we can apply Equation 8 and obtain p_{V_5} that can range from p_{neig} to p_{target}, depending on the α parameter chosen. In this particular case, α has a strong impact as if it is close to 0, priority is given to the neighbors, and the beige facies has poor chances of being drawn. In contrast, if α is close to 1, priority is given to the adjusted global proportions, which gives a great chance for the beige facies to be drawn. This is due to the over-representation of green and blue facies in Figure 2c compared to the global target proportions p^0_{global}.

2.4. Conditional Algorithm

We now consider the problem of conditioning the simulations. The conditioning data are facies intervals in boreholes as defined in Section 2.2. Considering any borehole,

$$B_i = (\mathbf{x}_i, \{z_1, \dots, z_m\}, \{k_1, \dots, k_{m-1}\}), \tag{9}$$

conditioning consists of ensuring that at least one surface must pass through each of the geological interfaces $(\mathbf{x}_i; z_j)$ observed in each borehole. Then, to condition the regions V_i with the proper facies, it is sufficient to ensure that no region covers two intervals having different facies.

The method that we propose to ensure the conditioning is described in detail in Algorithm 3. The method is direct and requires no iteration, but it requires checking at each step that it does not create situations that will lead to a violation of the conditioning data. This is the reason why the algorithm is complex. In the following, we explain the main principles of the algorithm.

Algorithm 3. Conditional Algorithm

Require: Same parameters as the Algorithm 1
Require: List of boreholes **B**
Order all the surfaces in **S** by their means
$d_s \leftarrow$ attribute a surface to each borehole facies transition and store it
Set surface index $t = 0$
$LB \leftarrow$ initialize lists for lower bounds conditioning
while $t < N$ **do** ▷ loop over the surfaces
  if S_t in d_s **then** ▷ If the surface is attributed
    $EP, UB \leftarrow$ Initialize lists for conditioning points (equality points and upper bounds)
  $B_i \leftarrow$ get borehole(s) and facies interval(s) associated with S_t
  Check situation at B_i according to Figure 3
  if Situation 1 **then**
    Set S_t to *onlap*
    $EP \leftarrow$ set an equality point to top of facies interval(s)
    $UB \leftarrow$ set upper bounds at other near boreholes locations to prevent connecting nonidentical facies (given Figure 3a)
  else if Situation 2 **then**
    Set S_t to *erode*
    $EP \leftarrow$ set an equality point to top of facies interval
  Compute one conditional surface with conditioning points EP, UB and LB
  Add EP to list of LB
  Remove facies interval of d_s
else
  Determine if S_t is *erode* or *onlap*, given ξ
  if S_t is *onlap* **then**
    Set LB and UB to prevent connecting two different facies as shown in Figure 3c
    Conditional simulation with LB and UB
  else

```
      Conditional simulation with only LB
  if S_t is onlap then
    t = t + 1                                   ▷ Increment time of deposition
    Apply Erosion Rules (Equations 3 and 4)
Define regions V_i as described in section 2.3.3
Assign facies to V_i using Algorithm 2
```

The surfaces are simulated from the bottom to the top. Surfaces can be onlap deposits or erosive as for the unconditional algorithms and they define regions. Because of their erosional capabilities, they can remove or cut parts of the regions that have been defined by previous depositions. The general aim of the algorithm is to ensure that in the end, no region covers two intervals having different facies in the boreholes.

This problem can happen in two situations: if the newly simulated region covers two (or more) intervals with different facies within the *same borehole*, or if the new region covers two (or more) intervals in *different boreholes*.

The first situation is avoided by forcing at least one surface to pass through each of the facies interface in each borehole as indicated above.

The second situation is more complex. It requires analyzing the position of the regions and intervals encountered in the different boreholes. As some surfaces have the potential to remove older ones by erosion, some situations that are compatible with the conditioning data at a certain time step may become incompatible with the data later on. The inverse is also possible. To solve this problem, the conditioning algorithm proceeds by generating the surfaces sequentially from oldest to youngest and uses inequality data (upper or lower bounds) to constrain the simulation. Three rules are defined and implemented in the algorithm:

A. For each interface point along each borehole with a facies transition, attribute a surface in **S** that has to go through that point; store this information in a data structure (a python dictionary) referred to as d_s. Note that one surface **S** can be attributed to one or several interfaces (in one or several boreholes).
B. When a facies interval is constrained (attributed to a region), we consider it untouchable and no *future* changes can alter it. This is done by imposing lower bounds (LB) along the borehole when simulating future erosive surfaces.
C. Onlap surfaces have to avoid creating (temporary) regions overlapping two different facies intervals to prevent the apparition of conditioning errors in the following steps.

To start, we generate N values within a uniform distribution between the minimum and maximum altitudes of the zone of interest. These values are ranked (step 1, in Algorithm 3) from minimum to maximum and will correspond to the mean altitudes of the N surfaces delimiting the regions.

Following rule R1, one surface is attributed to each interface (step 2, in Algorithm 3): for a given interface at elevation z, a surface S_t in **S** is chosen randomly according to a probability computed with a Gaussian distribution $\varphi_{\mu_t,\sigma_t^2}(z)$ of mean μ_t and variance σ_t^2, with μ_t being the prescribed mean elevation of S_t and σ_t^2 the prescribed variance of S_t. $\varphi_{\mu_t,\sigma_t^2}(z)$ is the probability that the surface S_t takes the value z at any location. Using this approach ensures that there is a reasonable chance that these transitions will be represented by a surface that is likely to be present at that depth. In addition, surface allocation ensures that surfaces associated with intervals in a borehole are of increasing index. This is to avoid the unrealistic situation where a younger interval is constrained before an older one. To do this, surface indices are randomly drawn, as described above until they are higher than the index previously drawn for the lower interval. At the end of the process, only a subset of the surfaces S_t are attributed to the interfaces observed in the boreholes. A surface can be assigned to several intervals of identical facies (below the interface). This is forbidden if the facies are different because there is a high risk of creating a region that would connect them.

The surfaces are then simulated successively.

If the current surface is attributed to an interface, several situations can arise. Figure 3 shows some of these situations. In the figure, the surfaces that have been simulated previously are represented in black and the intervals of the borehole data that have already been constrained by the conditioning algorithm and that should therefore

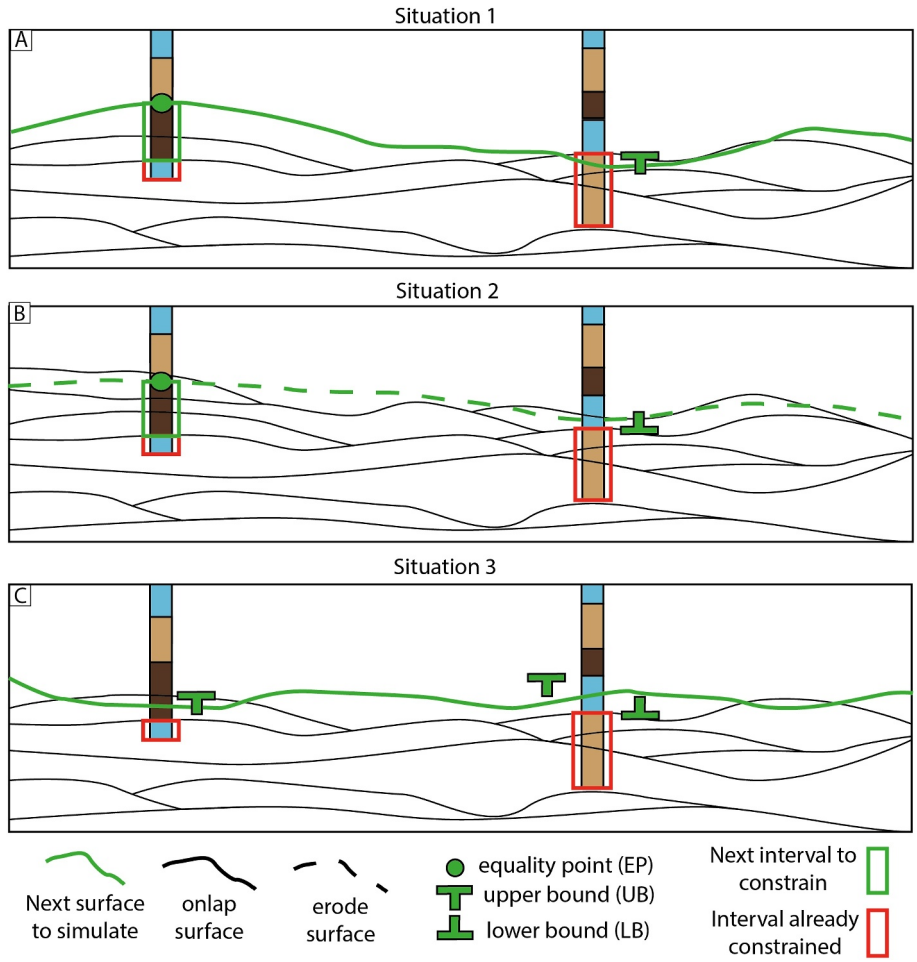

Figure 3. Three different situations can arise during the simulations of the surfaces. Situations 1 and 2 (a) and (b) concern a case where an interval has to be constrained while situation 3 (c) concerns onlap surfaces not constrained by an interface. See text for details. The horizontal bar of the "T" of the upper and lower bounds (UB and LB) is positioned at the altitude where the bound is applied. Note that these symbols are slightly offset to the left or right for better visibility. But they still apply to the borehole position.

not be perturbed anymore are highlighted with a red rectangle (rule R2). The new surface to be simulated is represented in green. In situations 1 and 2, the green rectangle highlights the current interval with a given facies that needs to be constrained during that iteration.

In situation 1 (Figure 3a), an onlap surface has to be considered. The current simulation elevation (last surface elevation, in black) at the well location (left well) is below the attributed interface. The green circle represents the position of the interface attributed to that surface (during step 2). It is a conditioning data, or equality point (EP) for the GRF simulation of this surface (step 12, in Algorithm 3). But the facies located above the already constrained interval in the second well (right well) is blue and therefore different from the facies in the left well (brown). To avoid creating a region that would connect these different facies, we impose in the right well an inequality (upper bound or UB) for the simulation of this surface (step 13, in Algorithm 3). We then use a Gibbs sampler (Freulon & de Fouquet, 1993) to constrain the conditional GRF simulation (step 17). After applying the erosion-deposition rules (step 29), the new region will cover only the brown interval in the left well in that case.

In situation 2 (Figure 3b), the current simulation elevation at the left well location is above the attributed interface. In this situation, an erosive surface has to be considered to ensure the removal of the previously simulated deposits. We add an EP at the interface (step 16). Then, to avoid breaking an interval that has already been constrained in other wells, we impose an LB constraint on the top of the intervals that were previously constrained (see right well with red rectangle in Figure 3b). We then use the GRF simulation technique with these new

constraints to generate the conditional simulation and apply the erosion-deposition rules as described above (steps 17 and 29).

The interval being now constrained, we can add the EP data to LB to prevent them being eroded by subsequent erosive surfaces (step 18) and interface is no longer attributed (step 19).

If the current surface is not attributed to an interface, We decide with a probability ξ if it is onlap or erosive (Step 21 in Algorithm 3). To prevent to connect different facies intervals, we add several constraints to onlap surface, as illustrated in situation 3 (Figure 3c). In this example the surface is forced to pass in the blue interval in the right borehole while avoiding the brown interval in the left borehole. The rest of the procedure is the same as before. Practically, this is done by randomly choosing a facies interval among the next to be constrained in each borehole and forcing the surface to pass through it using UB and LB, while avoiding other nonidentical facies intervals by applying UB. This prevents the connection of different facies.

The remaining steps (volume definition and facies assignment) are almost identical to the unconditional case. Before applying Algorithm 2, we simply attribute the facies from the boreholes to the regions that intersect them.

2.5. Hierarchical Workflow

Hierarchical structures are very common in Quaternary deposits (Miall, 1996). To model these features, one can apply EROSim within a hierarchical workflow. The hierarchical levels can be seen as the results of sedimentological processes at different spatial and temporal scales (or levels).

We consider these levels as sets of surfaces that separate not only lithofacies but also distinct sedimentological units. The basic principle is that a surface of a specific hierarchical level can only affect surfaces that have an equal or lower hierarchical level as discussed in Zuffetti et al. (2020). For example, a specific sedimentological body delimited by surfaces of a higher rank, cannot be eroded by a surface of a lower rank. From a computational point of view, this implies that we can simulate these deposits sequentially by hierarchical level from higher to lower levels.

For example, let us consider a case with two hierarchical ranks: one defined by surfaces having a large extent and delimiting large sedimentological units (or regions), and another one defined on a smaller scale with numerous surfaces frequently intersecting each other and producing regions of smaller sizes. To model this system, it is possible to decompose the simulation in two steps: first, high-order surfaces are simulated to delimit the boundaries of the different sedimentary units. In the second step, EROSim simulations are performed inside these units. Practically, this implies constraining the upper and lower boundaries of the simulation domain of EROSim with the simulated surfaces of the first. This can be extended to as many hierarchical levels as needed.

Using such a hierarchical approach, it is also possible to include more constraints in the model by setting different simulation parameters (α, ξ, N, surfaces interpolation parameters) for each unit or hierarchical level. But it implies inferring more parameters. The usefulness of the hierarchical approach is illustrated in Section 4.

3. Parameter Sensitivity

This section illustrates the EROSim capability to simulate a range of geometrical structures. We first present some unconditional 2D examples, as well as the effect of the different parameters (α, ξ, etc.) on the simulations (e.g., shape and size of the regions). We then demonstrate that the algorithm can be conditioned to well-data. Some 3D simulations are presented in Section 4 with a case study.

3.1. Unconditional Simulations

For most of the examples shown in this section, we consider a 2D vertical slice (x, z) of dimension 60×30 m^2 and with a spatial resolution of 0.33×0.15 m^2. We simulate a total of four facies ($k = 4$) in equal proportions. To keep things simple, we used the same covariance for all surfaces in a single EROSim simulation. However, there is no difficulty in using different covariance models. For example, a particular geological site may have a certain amount of erosive events that are distinct from the depositional events. In such cases, the erosive surfaces are likely to have a different geometry (e.g., smoother) and could therefore be modeled with an adapted covariance structure that has a higher correlation range and/or a smoother covariance model type, such as Gaussian covariance. In all simulations, the surface means are drawn from a uniform distribution between the top

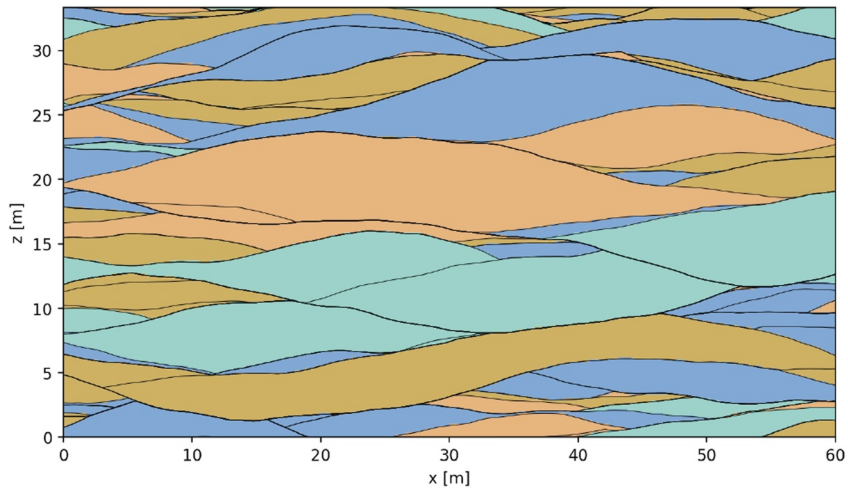

Figure 4. Example of an EROSim unconditional simulation with 100 surfaces. The four different colors represent four different facies. The black lines delimit the regions.

and bottom of the simulation domain. This allows distributing the surfaces uniformly over the domain and obtaining stationary simulations, but this is not a fixed feature of the algorithm.

Figure 4 shows one unconditional simulation with a stationary cubic covariance with a range of 45 m and a total variance of 5 m^2. The simulation parameters are $N = 100$ surfaces, 10% of erosive surfaces ($\xi = 0.1$), and the facies simulation being only driven by the marginal target probability ($\alpha = 1$).

Figure 5 illustrates the effects of the simulation parameters. As expected, the range of the covariance controls the geometry of the surfaces. A shorter range leads to rougher surfaces. But it also controls the size of the regions. A shorter range creates more intersections between the surfaces and leads to smaller regions (Figure 5a–5c). Logically, the number of regions also increases with the range. The proportion of erosional surfaces (ξ) does not modify significantly the size of the regions, but it changes rather their shapes (Figures 5d–5f). When there is no erosion ($\xi = 0$) the boundaries of the regions are mostly concave. This could correspond to a sedimentological situation dominated by the stacking of architectural elements such as gravel beds. But as ξ increases, more and more convex boundaries appear. This is the effect of erosion, which removes some parts of the regions that are filled later. This could correspond to a sedimentological situation with more energy that would result in a predominance of trough-like structures. As expected, the number of surfaces (N) influences the thickness of the regions (Figure 5g–5i), and their numbers. This is mainly due to our choice of drawing the surface means in a uniform distribution. The influence of the α parameter is also clearly visible (Figure 5j–5l). When α is equal to 0 (Figure 5j), the regions of the same facies tend to be clustered through the whole simulation domain, while when α is equal to 1, they are evenly distributed.

Different covariance models can also affect the shape of the regions. For example, Figure 6b shows a simulation with a spherical covariance model with a small range. The boundaries between the regions are rough, and they are more individual regions than with a larger range.

Figures 6a, 6c, and 6d illustrate the possibility of using non-stationary means or variograms through the simulation domain. In Figure 6a, the means are following a sinusoidal trend. In Figure 6c the means follow linear trends with varying slopes. And finally, in Figure 6d the sill and range of the variograms are progressively increasing to the right. These examples, even if they are a bit theoretical, show that if some information is known about the non-stationarity of the sedimentary structure, EROSim is capable of handling this information.

3.2. Conditional Simulations

In this section, we illustrate the capabilities of EROSim to produce conditional simulations based on borehole data. The number of facies is reduced to three in equal proportions. For all the examples, we used the same simulation parameters ($N = 100$, $\xi = 0.1$, and $\alpha = 0.5$). The surface means were randomly drawn from a

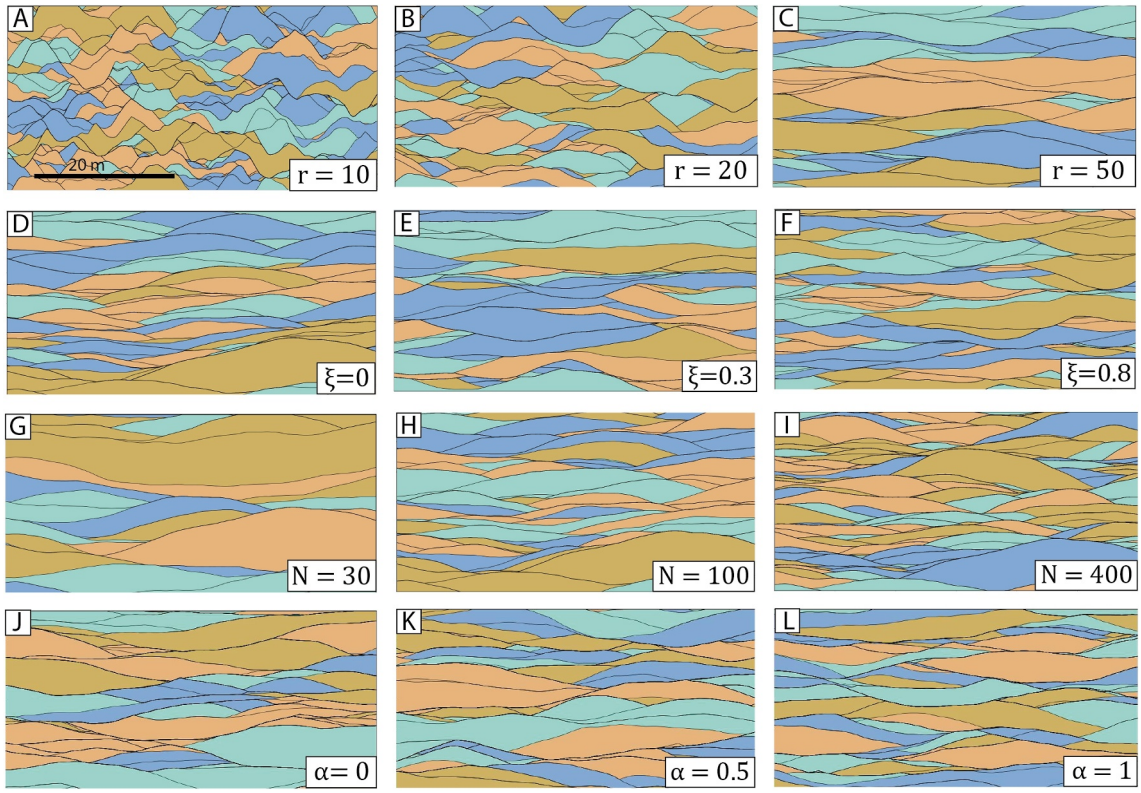

Figure 5. Different EROSim simulations where one parameter has been changed on each. (a–c) Simulations where the variogram range increases from 10 to 20 and then to 50. (d–f) Simulations where the ratio of erosive layer (ξ) increases from 0% to 30% and then to 80%. (g–i) Simulations where the number of surfaces (N) is modified, from 30 to 100 and then to 400. (J–L) Simulations where the α has been modified, from 0 to 0.5 and then to 1.

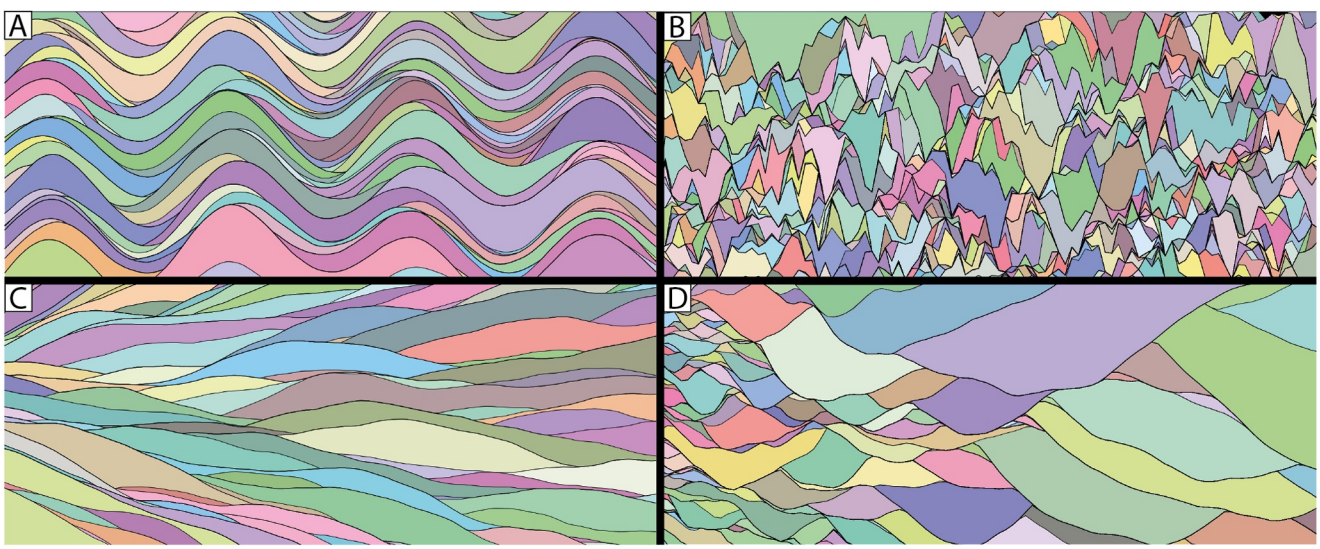

Figure 6. Realizations showing the capabilities of EROSim by varying different modeling parameters such as the mean (a), (c), the variance (d) or the covariance model (b, spherical). The different colors of the regions are just used to distinguish them.

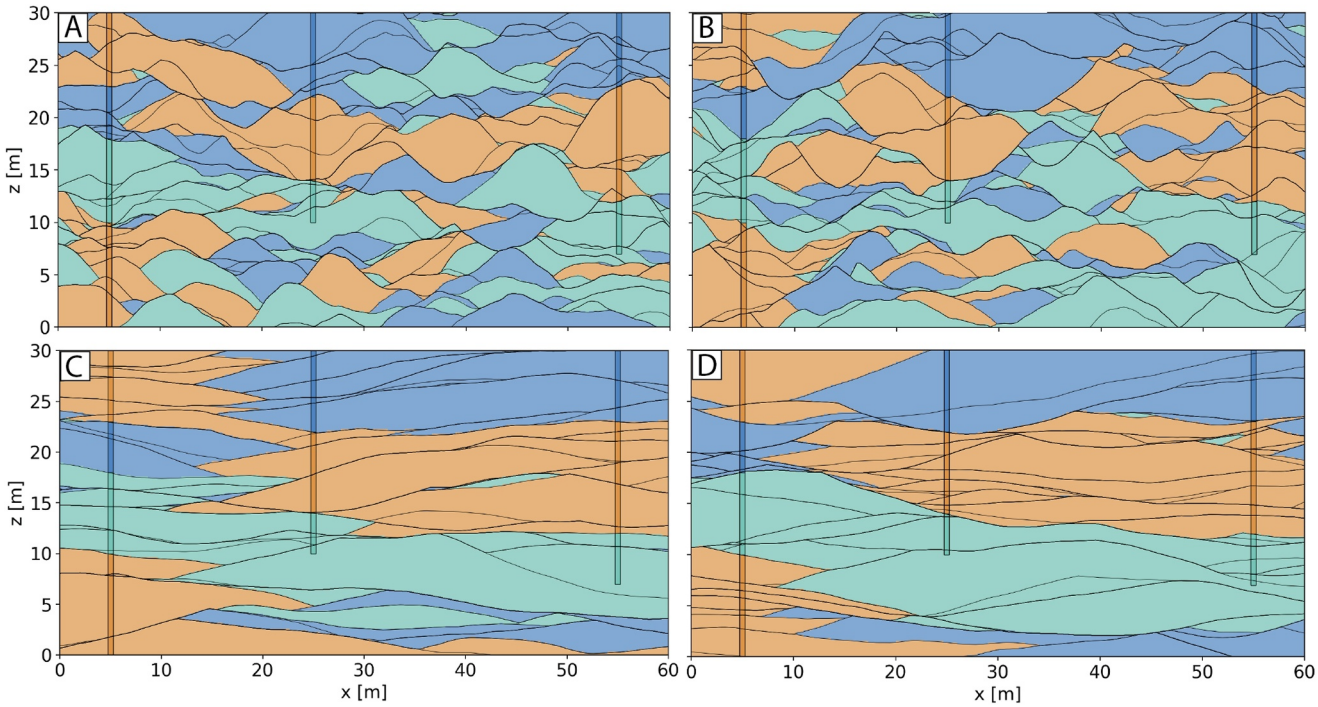

Figure 7. EROSim conditional simulations based on borehole data. (a) and (b) are two equiprobable realizations using a cubic covariance model with a range of 15 m and (c) and (d) were made with a cubic covariance with a range of 55 m.

uniform distribution between the minimal and maximal elevations. All surfaces are simulated with the same cubic covariance model with a sill of 5 m^2 and a range of 15 m or 55 m.

Figure 7 shows different conditional EROSim simulations using a range of 15 m (Figures 7a and 7b) or a range of 55 m (Figures 7c and 7d). The borehole intervals are correctly respected without any apparent deformation of the regions. Note that despite using the same value for the clustering parameter α (=0.5) for both cases, the facies regions are distributed differently. Realizations obtained with a variogram range of 15 m display more variability in the types of contact between the regions than the ones made with a variogram range of 55 m, since using the lower range results in a larger number of regions.

We used Sequential Indicator Simulations (SIS, Journel & Alabert, 1990) to compare EROSim capabilities against one of the most frequently used facies modeling techniques. Indicator variograms were estimated using EROSim simulations and used to produce SIS realizations. Four of those simulations are shown in Figure 8. SIS respects the conditioning data, proportions, and input variograms but does not succeed in reproducing some of the patterns (sharp contacts) proposed by EROSim. SIS produces more noisy and pixelized simulations with irregular facies boundaries.

If we compare the probability maps obtained by averaging 100 realizations (Figure 9), we observe similarities between the two methods. Indeed, the patterns of the facies probabilities are similar, except in the areas at depth not reached by the second and third boreholes. This is particularly obvious when the difference between SIS and EROSim predictions is plotted (Figures 10a and 10c).

Figure 10d highlights the differences in Shannon entropy (Shannon, 1948) between the two algorithms. The red area indicates a region where EROSim is more certain (less uncertainty) than SIS, while the blue area indicates the opposite (more uncertainty). This figure shows that SIS results are generally more uncertain (higher entropy) between the boreholes than EROSim. This is visible between the second and third boreholes (between $x = 25$ m and $x = 55$ m) which have nearly identical facies logs, implying a possible connection between the two. While EROSim is almost certain that a continuous connection exists between the two blue facies, SIS is not. The same comment can be made for the orange facies but the difference is not blatant. It can also be noted that the entropy depends on the choice of geostatistical parameters, as if the range of the variograms is too small (low horizontal

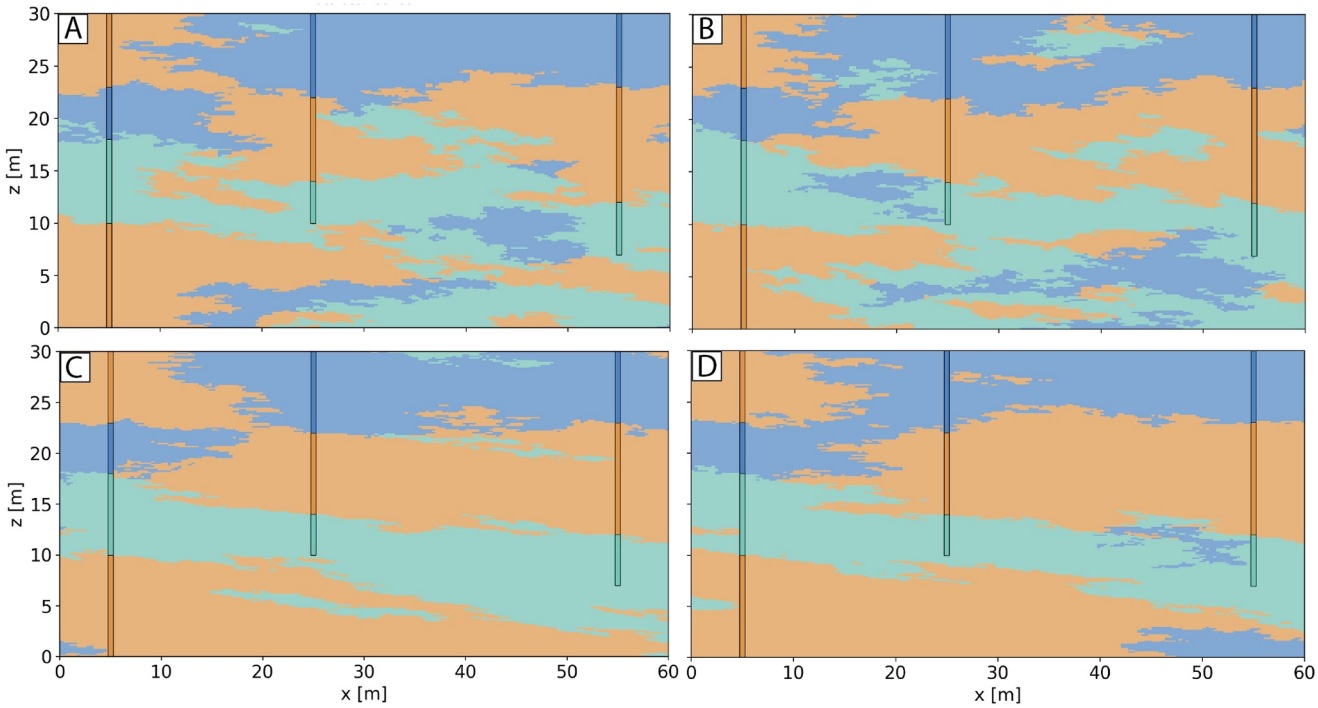

Figure 8. SIS simulations where each indicator variogram has been inferred from the corresponding EROSim simulations. Indicator variograms used to generate (a) and (b) were inferred on EROSim simulations with a range of 15 m (Figures 7a and 7b). Identical procedure was applied to generate (c) and (d) but on EROSim simulations with a range of 55 m (Figures 7c and 7d).

correlation), the models will be more uncertain (high entropy). In the comparison between SIS and EROSim in Figures 9g and 9h we can see that between the wells the SIS simulations have a higher entropy (high uncertainty) compared to the EROSim models. This is probably due to the difficulty in inferring correct correlation lengths for the variograms (the basis of the SIS models) in EROSim models. If the modeler has a general idea of the uncertainty, the Shannon entropy can be used as a constraint to properly select the geostatistical parameters.

4. Application to the Upper Aare Valley

In this last section, we illustrate the ability of EROSim to simulate structures similar to the ones observed in the field.

4.1. Study Site and Field Data

The study site is located in the Bümberg quarry (coordinates: 46°48′38.4″N 7°33′47.4″E), near Thun in the canton of Bern, in Switzerland. This site has been previously studied and described by Schlüchter (1973). Schlüchter et al. (2021) give a general description of Quaternary deposits in Switzerland and place the sediments from the Bümberg quarry in that broad framework.

This site has been selected because it is a suitable analog for the type of geological heterogeneity expected in the upper Aare Valley aquifer (Neven, Christiansen, & Renard, 2022; Neven & Renard, 2023). The quarry walls show fluvio-glacial Quaternary sediments made up of different sand and gravel facies that show complex relationships. This type of sedimentary architecture can be observed in many other sites in Switzerland and abroad.

To characterize its heterogeneity, the sedimentological structures, hierarchical levels, and deposits of the quarry walls were manually interpreted based on a field survey and a high-resolution photogrammetric UAV survey to obtain 3D ortho-normal images (Menga, 2021). This enabled the digitization of the delimitation and the characterization of the different stratigraphic boundaries and unit extents. In this quarry, Menga (2021) analyzed two walls, one oriented North-South (180 m long and 13 m high) and one oriented East-West (115 m long and 12 m high) to characterize the possible anisotropy of the sedimentological structures.

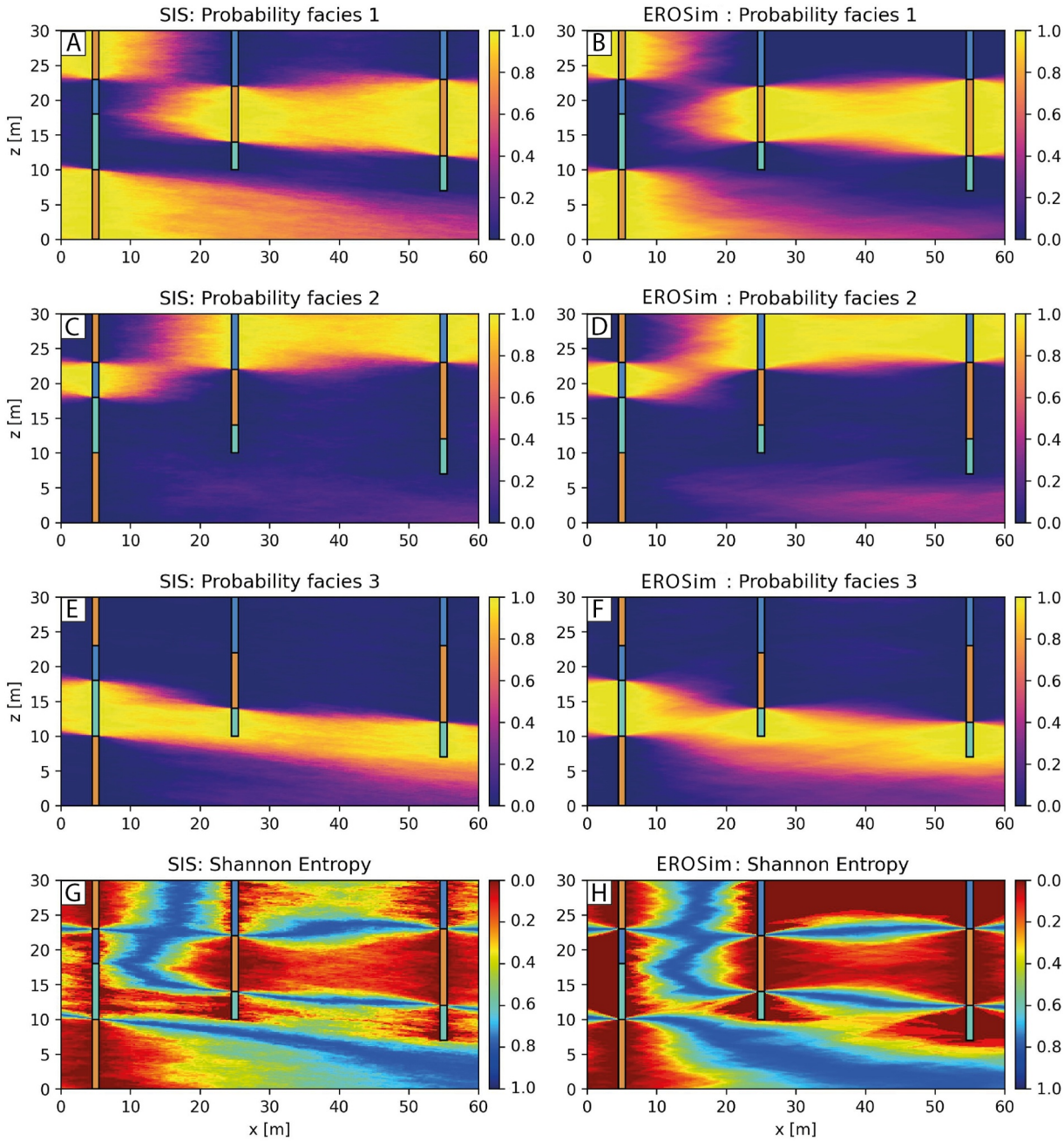

Figure 9. Probability of occurrence for each facies (computed over 100 realizations) considering a variogram range of 55 for EROSim simulations (Figures 7c and 7d) and SIS simulations made with variograms inferred on EROS simulations (Figures 8c and 8d). (a, c, e) are the probability maps for facies 1–3 for SIS method and (b, d, f) are the probability maps for facies 1–3 for EROSim method. (g) and (h) are the related Shannon entropy to probability maps for SIS and EROSim, respectively.

Several different lithofacies have been identified and described according to the classification proposed in Wentworth (1922) that takes into account the grain size and the sedimentological structures of the deposits. The different grain sizes are described by a capital letter: C (cobbles), P (pebbles), G (gravels), S (sands), and L (silts). The arrangement and/or the structure of the sediments are described by a lowercase letter: o (open framework), i (imbricated), h (horizontal stratification), n (normally graded), r (reverse graded), l (low angle stratification), p (planar-cross stratification), t (trough-cross stratification), s (draping troughs), x (cross-stratification), m (massive).

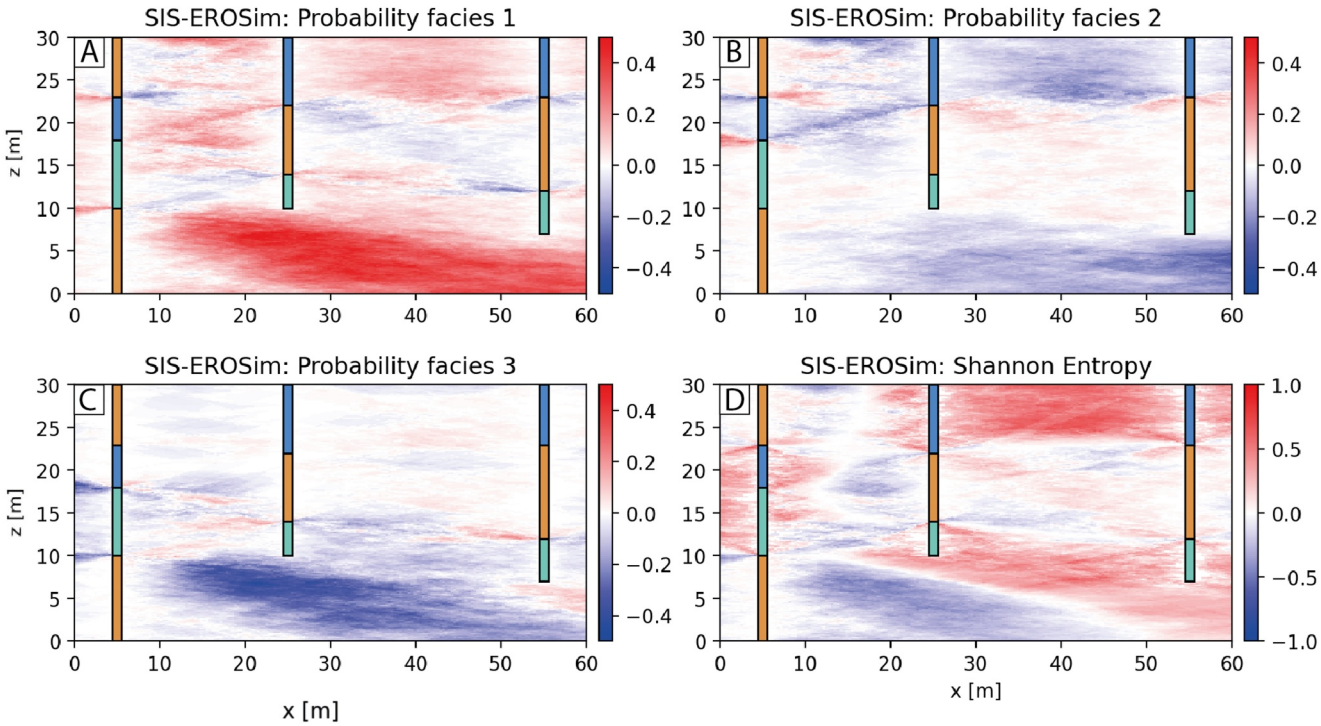

Figure 10. Plots of the differences between SIS and EROSim algorithms for the case shown in Figure 9 for probability of each facies (a–c) and Shannon entropy (d).

Menga (2021) regrouped them into seven facies groups and for each group a sedimentological origin interpretation has been proposed. These groups and interpretations are shown in Table 1 and Figure 11b shows the spatial organization of these facies on the East-West wall of the quarry. Gravel-dominated facies are the predominant groups of facies, whereas sand-dominated facies are quite dispersed and only present locally. Gravel facies are distinguished into four groups: bedload sheet aggradation (yellow), transverse bar migration (blue), scour fills (brown), and gravelly dunes (green), for a more comprehensive understanding of these sedimentological formations, please refer to Miall (1996).

In addition, six levels of sedimentological hierarchies have also been recognized, and named *Rank 1* (lowest rank) to *Rank 6* (highest rank). Figure 11a shows the interpreted surfaces on the wall of the Bümberg quarry. The surfaces of *Rank 1* to *Rank 2* are likely the result of very local processes (∼1–5 m) while *Rank 3* surfaces have a larger extent (∼5–60 m). Higher-order surfaces (*Rank 4–Rank 6*) exceed the size of the domain and can be treated equally in this situation. There are a total of six of these surfaces on the two walls, which delimit five sedimentological bodies (Units in Figure 11a) that differ in terms of facies proportions and structures.

Table 1
Facies Code and Their Interpretation in the Bümberg Quarry

Facies code	Interpretation	Facies color
C,P,G(h,l,n,i,m)	Bedload sheet aggradation	Yellow
C,P(p,t,x)	Transverse bar migration	Blue
C,P,G,Ss	Scour fill	Brown
PS,GS(p,t,x)	Gravelly dunes	Green
SG,S(p,t,x)	Sandy-gravelly dunes	Dark Green
SG,Sh	Sandy wedges	Pink
SH,S(l,m)	High flow regime sandy levels	Orange

Note. The colors used to represent them are also given.

4.2. Model Setup and Parameters

To account for the hierarchical relations observed on the study site, we consider the hierarchical approach proposed in Section 2.5. At the lowest rank, the regions are filled with facies while surfaces of higher ranks are simulated independently to delimit stratigraphic units. For the upper Aare valley, the aim is to produce a model of lithofacies. Based on the field observations, we consider that it is reasonable to set the lowest rank to *Rank 3* surfaces (Figure 11a, yellow lines) and to fill the delimited regions with the facies that are mostly differentiated by these surfaces. Figure 11b shows that these are gravel-dominated facies. The sand facies (dark green, pink, and orange) are more dispersed and often delimited by surfaces of *Rank 1* or *2*. Therefore, we must consider as well the hierarchical levels above *Rank 3* (pink, blue and red surfaces). Furthermore, the regions delimited by these higher rank surfaces have different characteristics in terms of sedimentary

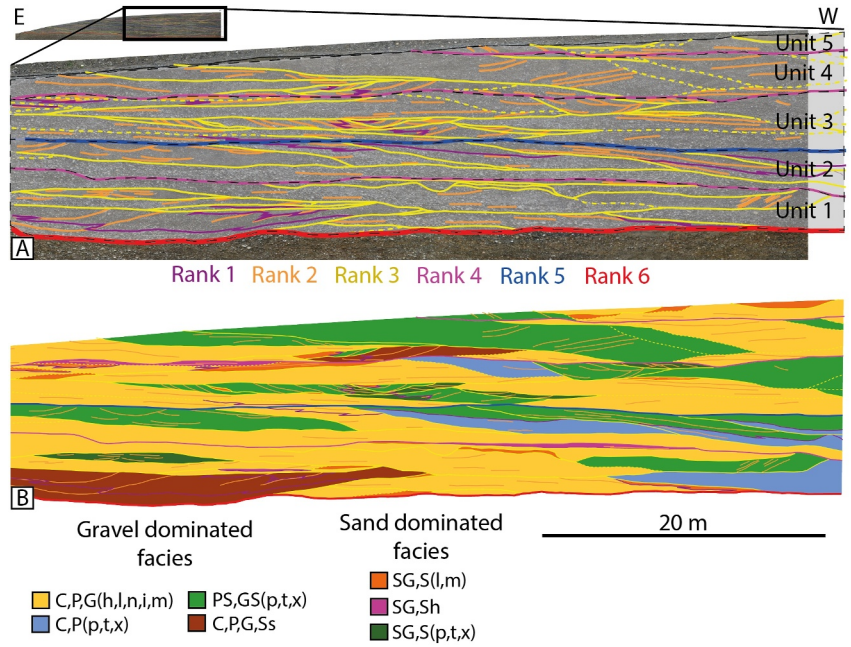

Figure 11. Interpretation of a part of the East-West wall of the Bümberg quarry realized by Menga (2021). (a) is the reconstructed image of the wall acquired by the drone as well as the sedimentological surfaces that separate the subfacies bodies. The hierarchical rank of each surface is given by its color. The five stratigraphical units, delimited by surfaces of rank 4 or higher are also shown. (b) shows the corresponding colorized facies groups interpretation. For readability and clarity, only half of the wall is shown. Figures and data are taken and modified from Menga (2021)).

body sizes and facies proportions. Finally, we only simulate the four dominating facies (mainly gravels). Orange and pink facies have been regrouped into the yellow facies, while the dark green facies has been regrouped with green facies.

As explained in Section 2.5, the approach is decomposed into two steps. First, the geostatistical parameters of the higher-rank surfaces are required to define the extent of each unit. From base to top in this quarry, Menga (2021) recognized a first unit bounded by a surface of *Rank 6* and *Rank 4*, a second unit bounded at the top by a *Rank 5* surface, a third, fourth and fifth units, bounded at the top by *Rank 4* surfaces (Figure 11a). Consequently, it is required to simulate three *Rank 4* surfaces and one *Rank 5* surface. Therefore, for each wall, the variograms for *Rank 4* and *Rank 5* were estimated on the available surfaces as well as the mean altitudes of each of the surfaces. The parameters to model those surfaces are provided in Tables A1 and A2 in Appendix A. *Rank 6* surface was not modeled and was simply considered to be the bottom of the simulations.

In this phase, we undertake the simulation of *Rank 3* surfaces within each distinct unit. EROSim requires that we infer the following parameters: the number of surfaces (N), a distribution for the mean altitudes of the surfaces, the variogram models of the surfaces (μ_i and γ_i), the proportion of erosive surfaces (ξ), the proportions of the facies (p_{global}), and lastly, the clustering parameter (α).

The γ_i were estimated using the interpreted surfaces, drawn by Menga (2021), by computing the experimental variogram on each independent line (or surfaces) and by adjusting a variogram model on them. Note that we only considered lines with a minimal length of 5 m to obtain representative statistics. The spatial statistics of these surfaces for the EW Bümberg wall are summarized in Figure 12 for each unit. Unit 5 is not represented, as there were not enough surfaces to infer proper variogram models. In this case, we used the mean values of the parameters, and averaged on all the variogram models. Finally, for each unit, the inferred parameters of the variogram models were averaged to keep only one set of parameters.

The other parameters (N, ξ, p_{global}, α) were estimated by trial and error and are given in Table A3 in Appendix A.

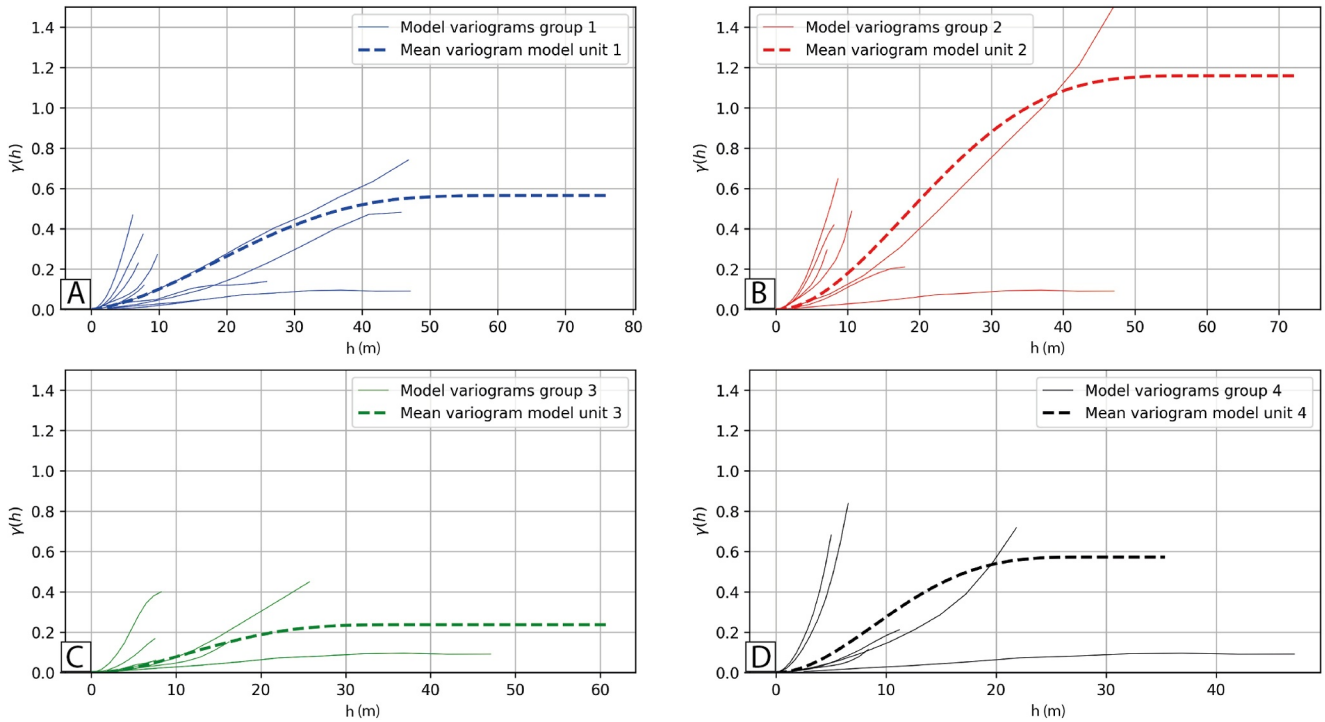

Figure 12. Experimental and fitted model variograms realized on the EW wall of the Bümberg quarry for each different unit. (a) Variograms for unit 1, (b) Variograms for unit 2, (c) Variograms for unit 3, (d) Variograms for unit 4.

4.3. Heterogeneity Models in 2D

Figures 13 and 14 show EROSim simulations of the quarry walls and the observed geology for the same locations. For comparison purposes, Table A3 gives information about the facies proportions in each unit for each different Quarry wall. Generally, the simulations reproduce rather well the shapes of the regions as compared to the reference. A more quantitative analysis of the results has been conducted on an ensemble of 100 realizations for the two sections. It shows that the indicator variograms computed for each facies for each EROSim simulation are well distributed around the reference indicator variograms, as illustrated in Figure 15a–15c for N-S wall. The proportions are also well respected (Figure 15d). Similar results are obtained with the E-W wall.

To test the capabilities of the conditioning algorithm (Section 2.4), four boreholes were extracted from the reference and used to constrain EROSim simulations (Figure 16). Compared to the unconditional simulations (Figures 13 and 14), the conditional simulations are closer to the reference, thanks to the borehole information.

In general, the previous examples show that the 2D cross-section models demonstrate a high degree of similarity with the reference data set. Additionally, the models appear to have difficulty in accurately reproducing specific patterns, such as the vertical succession of certain facies (e.g., the blue-green sequences that are frequent in the original data in Figure 13d). The main reason for this is the simplicity of the facies assignment step of the EROSim approach, where facies are assigned based only on simple facies proportions and neighboring regions. More complex approaches to calculating probabilities, such as transition probabilities, could be considered. This would require additional work to modify the algorithm to accommodate such approaches.

4.4. Flow and Transport Simulations

To push the comparison further and assess the capability of EROSim to reproduce not only the observed sedimentary structures but the features that are relevant to model groundwater flow and transport accurately, we performed 2D flow and transport simulations within the area delimited by the red rectangle area shown in Figure 17a. This experiment aims to evaluate the ability of EROSim to generate sedimentological structures that have the same effect on the flow field as the observed sedimentological structures. As a reference, we use the east-west wall of the Bümberg quarry. SIS simulations were performed for comparison purposes as before.

10.1029/2024WR038364

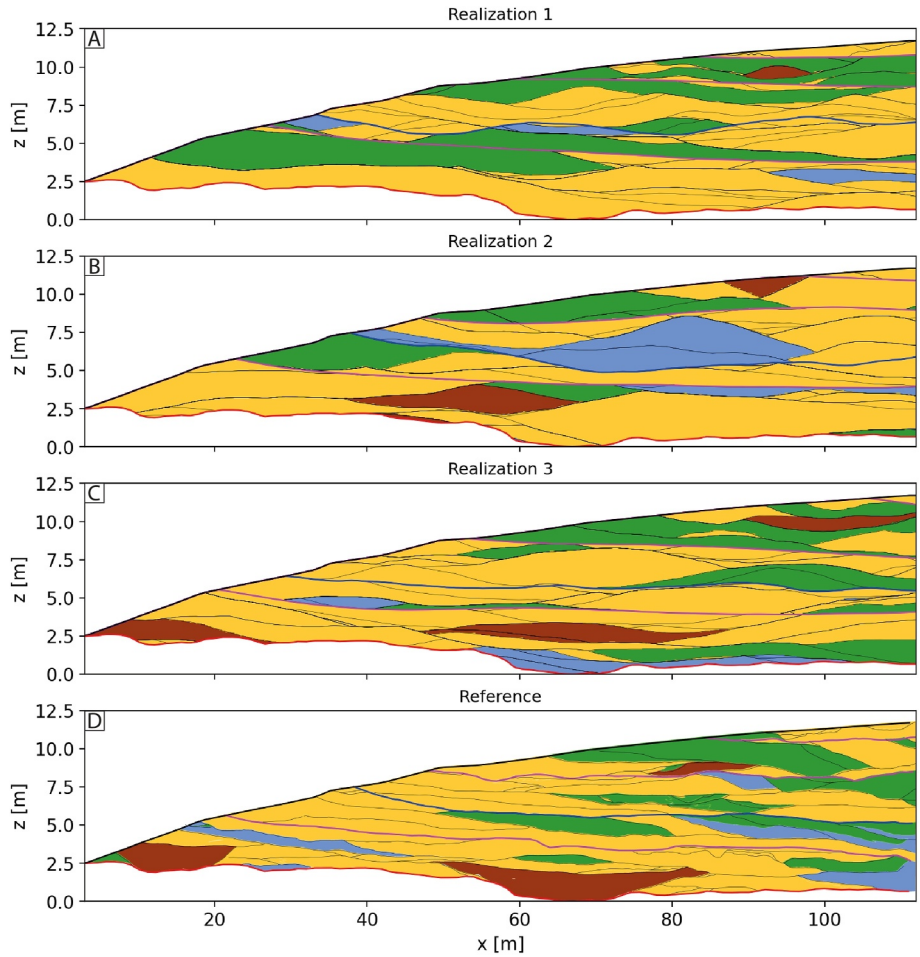

Figure 13. Three EROSim simulations of the East-West wall of the Bümberg quarry (a–c) and the interpreted wall made by Menga (2021) considered as the reference (d). The sedimentological lines that separate the regions are not shown.

The groundwater flow model was built using MODFLOW 6 (Langevin et al., 2017), the particle transport was computed with Modpath 7 (Pollock, 2016). Everything was coded and scripted with the FloPy python package (Bakker et al., 2016). The model is a vertical 2D section model of 125 × 154 cells (number of layers × number of cells in *x*-direction). The cells have a constant thickness of 0.0625 m and a constant width of 0.39 m, resulting in a model of 7.81 m × 60 m in total length and 19'250 cells. The left and right boundaries of the model were set to constant head (0 m on the left and 1 on the right, which implies an hydraulic gradient of around 0.015), while the upper and lower boundaries were assumed to have no flow conditions. The model is run in steady state, so only hydraulic conductivity (K) values are considered. The mapping between the geological models (EROSim) to the groundwater model (MODFLOW 6) was simply made by using same grid for both models and assigning hydraulic conductivity values to each corresponding facies. Each facies was assumed to be homogeneous and isotropic (Kxx = Kzz). Therefore, model cells belonging to the same facies were assigned a unique K value (Figure 17a). Fifty realizations of EROSim and SIS were generated, and the same procedure was applied to transform the facies to continuous K fields. The realizations are conditioned on two boreholes. The SIS parameters were inferred from the reference directly. The choice of the K values is consistent with the nature of the sediment types and was chosen to ensure a significant contrast. It is not based on actual measurements which are unavailable for the site. The goal is to test the ability of EROSim to simulate the sedimentological structures of a reference and to compare it with a standard method (SIS).

For the advective transport simulation, a total of 96 particles were released uniformly at the right boundary cells in the model between layers 15 and 111. An homogeneous value of 0.3 was considered for the porosity over the

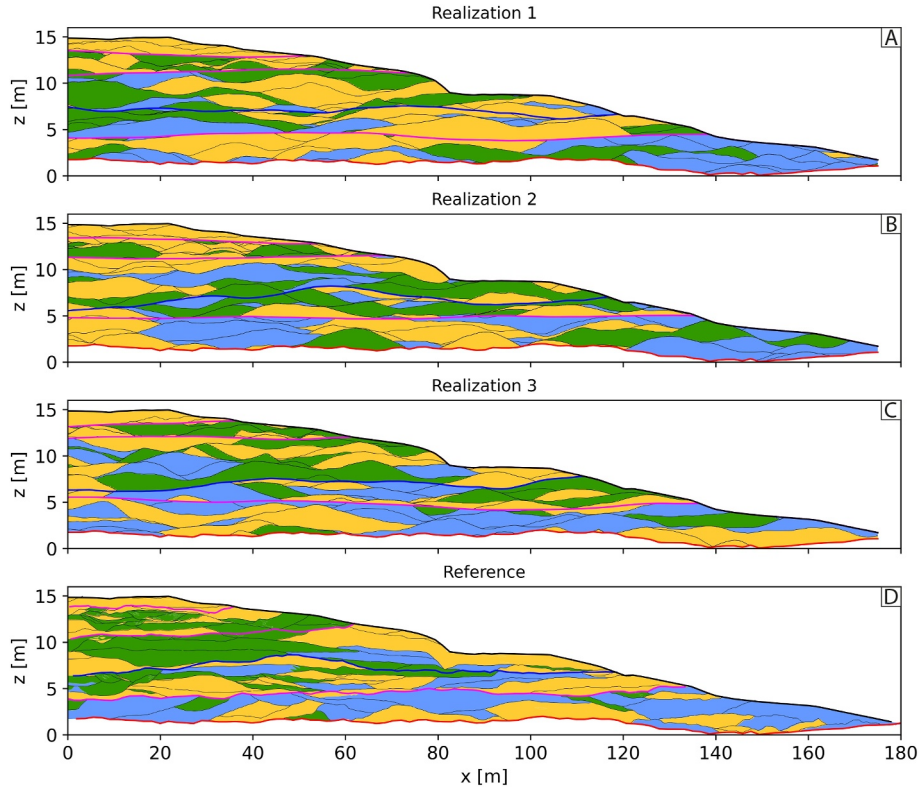

Figure 14. Three EROSim simulations of the North-South wall of the Bümberg quarry (a–c) and the interpreted wall made by Menga (2021) considered as the reference (d). The sedimentological lines that separate the regions are not shown.

simulation domain. Each particle was placed in the center of each cell. Figures 17a–17c show the flow paths of the particles in the reference, one EROSim simulation, and one SIS simulation, respectively.

The results obtained from the 50 simulations are summarized in Figure 17d. It depicts the distribution of the cumulative number of particles that reached the left boundary of the model as a function of time for the 50 realizations. This figure allows comparing the results of the EROSim and SIS simulations (shown in blue and red, respectively) against the reference (shown in black). First of all, we observe the wide range of the predictions for both methods, indicating a high degree of uncertainty because the heterogeneity models are conditioned only on two wells. We also observe that the median arrival time obtained with the EROSim simulations is much closer to the reference than the median obtained with the SIS simulations. In addition, we have calculated the Root Mean Square Errors for each curve (compared to the reference), resulting in 50 RMSE values for SIS models and 50 RMSE values for EROSim models. The mean RMSE for EROSim simulations is 13.4 (in number of particles) against 16.3 particles for SIS simulations. All of this seems to indicate that EROSim was able to better reproduce the sedimentological structures of the reference that control flow and transport as compared to SIS.

4.5. Heterogeneity Models in 3D

EROSim can also be used to generate 3D heterogeneity models. Figure 18 shows such 3D simulations using the sedimentological statistics inferred on both walls of the Bümberg quarry. Standard parameters (Table A3) have been averaged between the two walls, as well as the altitudes of the surfaces of the higher ranks. The 1D variograms were also combined to obtain 2D variograms for the surface simulations. This was done by assuming that the spatial statistics inferred on the walls represent the statistics on the major and minor axes of anisotropy of the 2D variogram. The variogram ranges on the NS wall were assigned to the range on the Y axis of the 2D variograms, and the variogram ranges on the EW wall were assigned to the range on the X axis. Sills were averaged. The grid used for the visualization has a cell size of $0.85 \times 0.85 \times 0.14\ m^3$ and contains $100 \times 100 \times 100$ cells.

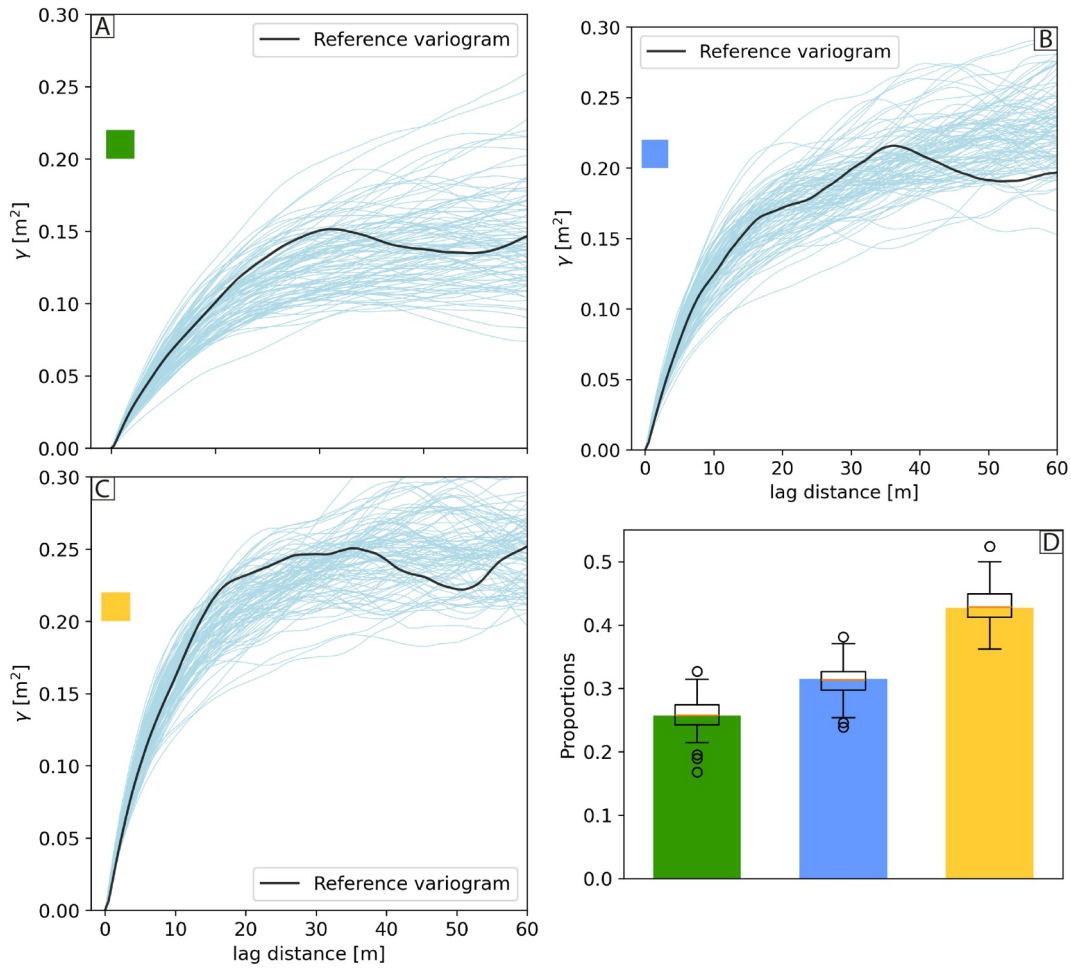

Figure 15. (d) Comparison of proportions where each colored bar represent the facies proportions in the reference and the boxplot the distribution of these proportions among the realizations. (a–c): Indicator variograms for each facies between the references and 100 realizations of the N-S wall.

Figure 18 shows significant variability between the realizations because of the absence of conditioning. It also shows that EROSim can reproduce the expected shapes of the sedimentological structures while exploring a broad variety of plausible configurations. The sedimentological lines bounding the regions are not shown here for the sake of visibility, but it is important to remember that this additional information is available. Regions can be individualized and treated differently in successive modeling steps (e.g., simulation of physical properties).

A possible use of the 3D geological simulations is to link the detailed heterogeneity mapping at the outcrop scale and the distribution of equivalent hydraulic conductivities to be used in groundwater flow models at a regional scale. To illustrate this possibility, the hydraulic conductivity tensors have been computed for all the 3D simulations presented above. There are many approaches for computing the equivalent hydraulic conductivity tensor (Renard & Ababou, 2022). Here we use a numerical technique capable of identifying the full tensor. The flow simulations are carried out with Modflow 6. For each flow simulation, linearly varying heads are prescribed on all the faces of the 3D block to impose the head gradient in a given direction. Three flow simulations are performed, one with the head gradient along the x axis, one along the y axis, and one along the z axis. For each simulation, the three components of the Darcy flux vector are averaged within the domain and used to calculate the equivalent conductivity tensor using Equation (94) from Renard and Ababou (2022).

The calculation is repeated for the 50 3D simulations (such as the one shown in Figure 18). To remain consistent, the local hydraulic conductivity values are the same as those used for the 2D transport simulations. Indeed, we do not have direct measurements of the hydraulic conductivities of the facies mapped in the quarry.

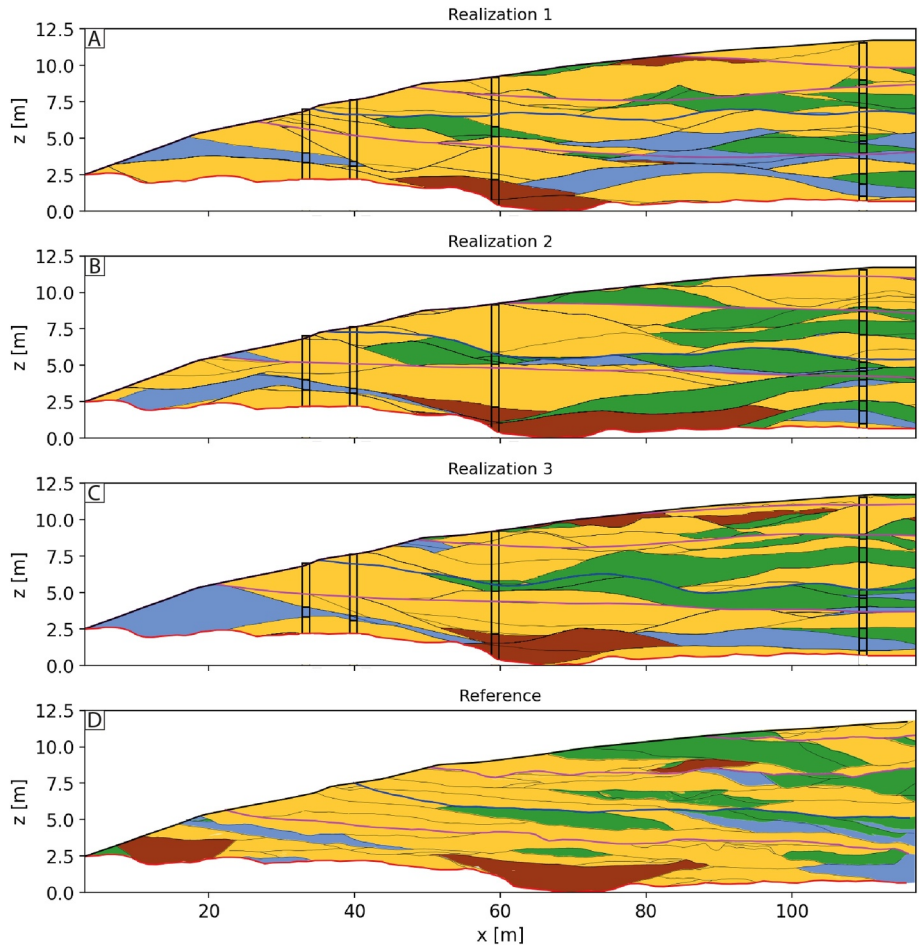

Figure 16. Three conditional EROSim simulations of the East-West wall of the Bümberg quarry (a–c) and the interpreted wall made by Menga (2021) considered as the reference (d).

To represent the results, the 50 tensors were decomposed into eigenvalues and eigenvectors shown in Figures 19a and 19b respectively. The eigenvectors show the principal directions of anisotropy. The first and second directions of anisotropy are within the horizontal plane and fluctuate slightly around the x and Y directions. The third direction is instead very stable and is along the vertical axis. The eigenvalues (Figure 19a) show that conductivity along the X direction is slightly larger than along the Y direction. We interpret this difference as a result of a slight difference in the geometry of the sedimentological patterns along the X and Y directions. However, the most important anisotropy contrast is observed when comparing the eigenvalue along the Z direction and the two horizontal directions. The anisotropy contrast is larger than 10. With the hydraulic conductivity values that were chosen for the different facies, the resulting anisotropy factor is consistent with values published in literature (Bakker & Bot, 2024).

5. Discussion

In this paper, we presented EROSim, a novel surface-based simulation method and a conditioning algorithm that can represent sedimentological heterogeneity that is frequently observed in fluvio-glacial systems.

5.1. Parameterization

Overall, an important advantage of the presented approach is that it can generate multi-facies simulations with a reduced number of parameters as compared to existing methods. Only five groups of parameters are required: the marginal distribution of the facies (i.e., their proportions p_i), the number of surfaces (N), a single variogram for all the surfaces, the ratio of erosive layers (ξ), and the clustering parameter (α). Most of these parameters can be

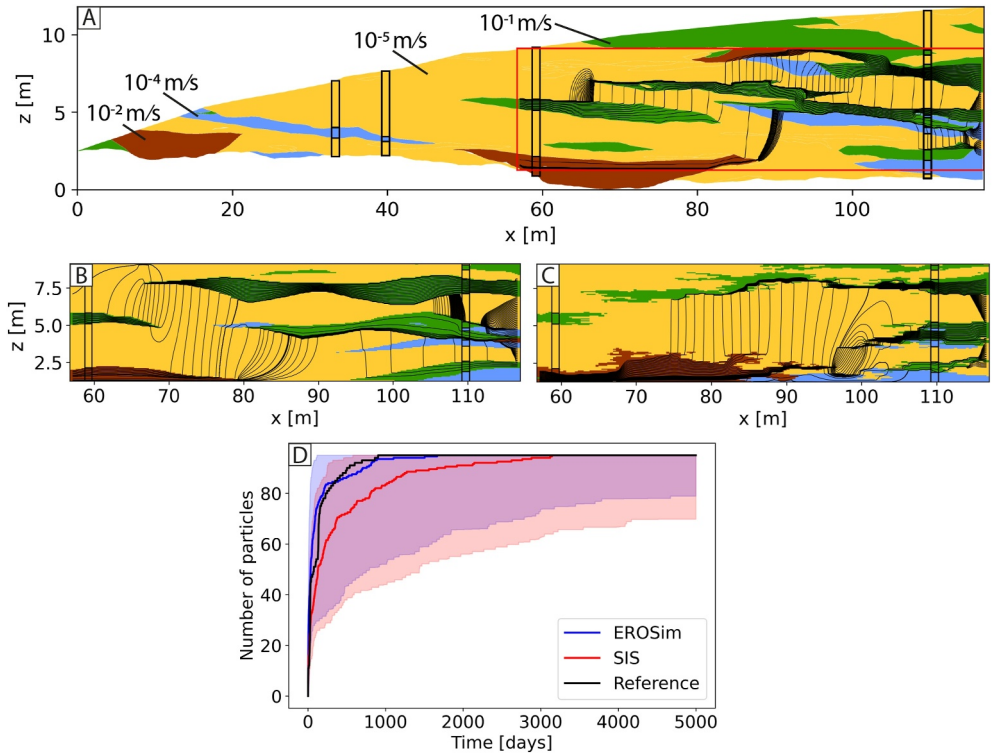

Figure 17. Flow and particle transport. (a) shows the observed (reference) facies distribution along the East-West wall of the Bümberg quarry and the paths of the particles obtained by assuming a gradient from right to left. The hydraulic conductivity values assigned to the different facies are also shown. (b) and (c) show the particle flow paths on one of 50 of the EROSim and SIS realizations, respectively. The shaded areas in (d) represent the range (10%–90% quantile) of the cumulative number of particles reaching the left side of the model as a function of time for all realizations for both EROSim and SIS. The solid lines represent the median, while the black solid line represents the result obtained on the reference.

inferred from accessible data. The facies proportions can be derived from borehole observations, as well as the number of surfaces. The variogram can be estimated from outcrop studies. It may be difficult to estimate if only borehole data are available but then its physical interpretation is simple (the sill of the variogram controls the vertical span of the fluctuations of the stochastic surfaces and the correlation length controls their lateral extension. One can therefore provide reasonable estimates based on common sense or observations in analog sites. The ratio of erosive layers can be used to adjust the expected geometry (more superposition of sediment structures such as gravel beds when ξ is close to zero, and more troughs when ξ is close to 1) if this information is available. Similarly, the value of α can be adjusted depending on available information on outcrops. If no obvious information is available to estimate these parameters, they can be estimated by conducting K-fold cross-validation as shown for example, in Juda et al. (2020), and by optimizing a quality criterion such as the continuous rank probability score (CRPS). Following this approach, data (e.g., boreholes) are separated into K different groups (folds) and K-1 groups are used as constraining data, while the last group is used as a test data to validate the results. This operation is repeated K times, where each fold is successively the test data group. In the end, it is possible to assess which set of parameters give the best predictions on the test groups. Having a reduced number of parameters facilitates their identification.

As a point of comparison, for a simulation including four facies, the EROSim simulation method requires eight parameters (three proportions from which four can be expressed: $p_1, p_2, p_3, p_4 = 1 - p_1 - p_2 - p_3$, a variogram type, sill, and range, ξ and α). The SIS method requires the facies proportions and four variograms. This leads also to a total of around eight parameters depending on the complexity of the variograms. Concerning the TPROGs software (Carle, 1999), it also requires the proportions, but in addition, it needs the probability of transitions for each facies and for each couple of facies. The number of parameters is therefore higher than for EROSim and SIS. If we consider an object-based, rule-based model, or process-based model the number of parameters is usually

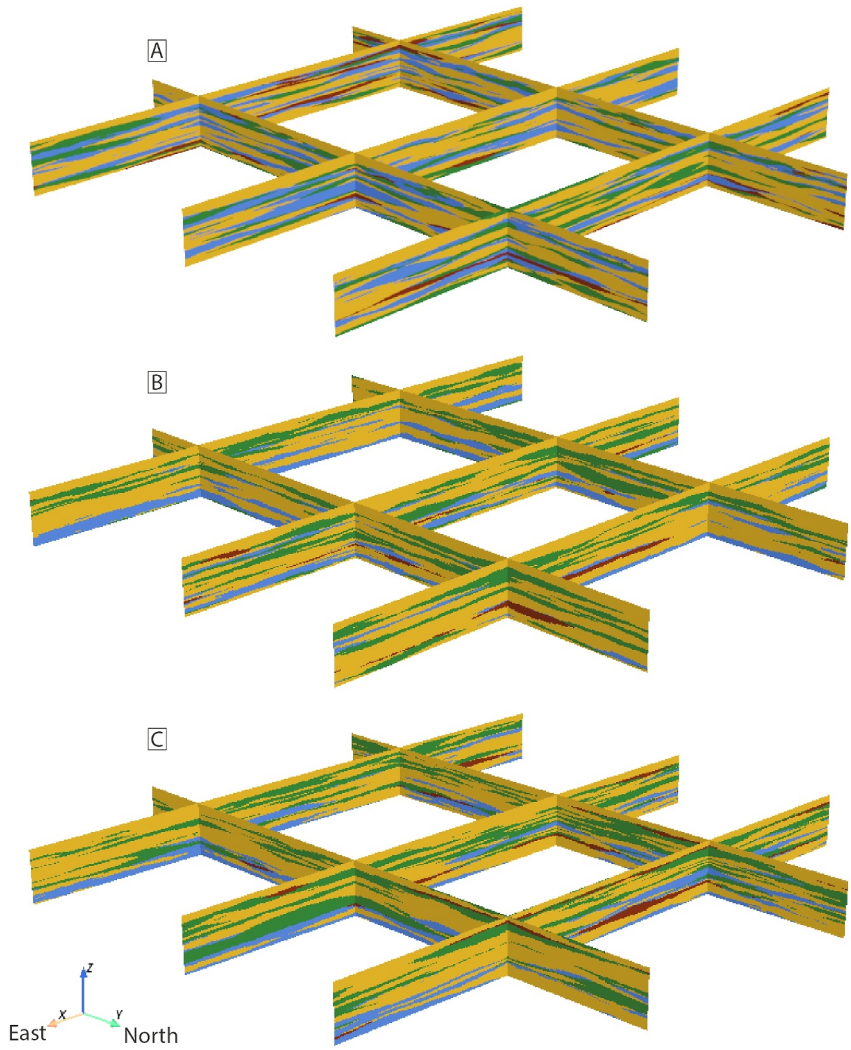

Figure 18. Three different realizations (a–c) of EROSim 3D simulations of the Bümberg quarry. The model dimensions are 170 m × 170 m × 14 m, there is no vertical exaggeration.

much higher because all the statistics concerning the geometry of each architectural element and the relations between them or the underlying physical processes have to be quantified.

5.2. Application on Real Data

The application of the EROSim method for the Bümberg quarry site demonstrates that the results obtained with this method represent reasonably well, for such a parsimonious model, the main sedimentological features observed on the quarry walls. This is also confirmed by the flow simulation experiments (Section 4.4). The particle transport results are closer to the reference with EROSim than SIS. In this example, the particles tend to arrive earlier with EROSim than with SIS models (Figure 17d). This result could be explained by the noisy aspects of the SIS models that could affect the connectivity. It is important to note that the uncertainty remains large both for SIS and EROSim, highlighting the difficulty of reproducing precisely the complex architecture of the quarry wall.

Some differences concerning both the shape of the regions and the distribution of the facies are visible on Figures 13 and 14. The greatest discrepancy between the reference and the simulations is that the surfaces delineating the regions exhibit a higher degree of variability in the reference than in the simulations. This discrepancy is likely due to the use of a single variogram to model all internal surfaces. Indeed, Figure 12 shows a

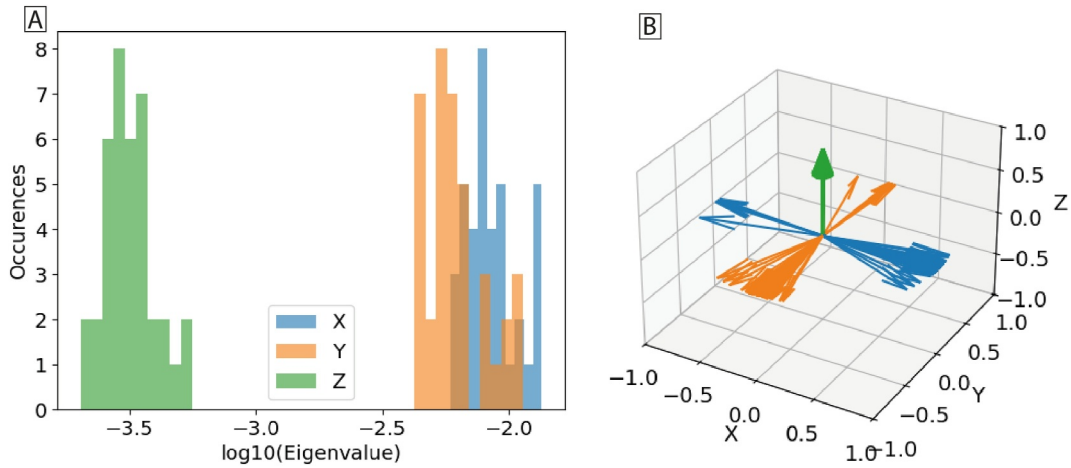

Figure 19. Summary of the eigen values decomposition of the equivalent hydraulic conductivity tensors obtained on 3D realizations of the Bümberg quarry. Note that each color represents a specific axis. (a) Histograms of eigenvalues. (b) 3D view of the eigenvectors.

large spectrum of estimated variogram models from the field data, regardless of the unit. The use of a single variogram model cannot capture all this variability. Modeling the interfaces with different variograms is possible but it would make the parameterization more complex, but we consider that it would not necessarily be useful or critical for groundwater applications. This is also suggested by the results of the flow simulations.

5.3. Link With Sedimentological Structures

As compared to other facies simulation methods, and as we discussed in Section 5.1, EROSim provides a very parsimonious control over the geometry of the geological interfaces. The sensitivity analysis (Figure 5) shows that depending on the value of ξ different types of architectural elements can be obtained, but the model is not constructed to provide a strong control on these architectural elements. Compared to object-based (Bennett et al., 2019; Haldorsen & Lake, 1984; Rongier et al., 2017), Multiple Point Statistics (Mariethoz et al., 2010; Strebelle, 2002), rule-based (Pyrcz et al., 2015; Ramanathan et al., 2010; Scheibe & Freyberg, 1995), or process based models (e.g., Koltermann & Gorelick, 1996; Koneshloo et al., 2018), the possibility to generate specific sedimentological structures such as meanders, bars, or levees (Miall, 1996) is much weaker with EROSim. This is a limitation of the method and therefore its domain of application is different. But, one main advantage of EROSim is that it does not require sophisticated inputs, such as a training image for MPS or the definition of geological objects and their spatial relations for OBM.

Another major advantage of EROSim is that it can easily be conditioned. The most sophisticated methods listed above are difficult to condition with borehole data for two reasons. The first is the complexity of the conditioning algorithm. Many of the advanced facies simulation methods cannot yet be fully conditioned. The second reason is more fundamental. In many situations, the type of architectural elements that can be inferred from outcrops or geophysical data sets (e.g., GPR) cannot be identified in boreholes (Miall, 1996). But, boreholes constitute the vast majority of the available data. Having a sophisticated method that represents properly the architectural elements but that cannot be fed with the proper conditioning data in boreholes is a limitation of these advanced methods. With EROSim, we do not assume that detailed data about the types of sedimentological architectural elements would be available on boreholes. We only rely on the level of information that is available (rock types). For all these reasons, we prefer to keep the model very simple. It ensures its applicability to readily available data sets.

Nevertheless, EROSim provides a representation of the boundaries between the elemental volumes that can help define simple internal structures within single facies. Given the simulated surfaces, a possible extension of the method would be to compute locally the slope of the underlying or overlying surfaces and use it to estimate varying orientations within each region. This could be used to orient local anisotropy tensor following for example, the method that was presented by Borghi et al. (2015). This principle could be used to represent in a

simplified manner cross-bedding structures within the regions. The simulated surfaces offer also a possibility to extend the model by defining thin and continuous structures of fine sediment deposits such as clay drapes at the bottom of some architectural elements. This possibility has not been explored in the paper, but clay drapes are known to have an important influence on flow and transport (Huysmans & Dassargues, 2012) and are difficult to simulate with other approaches.

5.4. Algorithmic Limitations and Possible Extensions

Some further limitations and possible extensions of EROSim have been identified. The conditional algorithm requires imposing rules on the simulation of surfaces. This is permitted thanks to the use of inequality data when modeling Gaussian Random Fields, and this is one of the main novel contributions of this paper. In most cases, the conditioning does not perturb the shape of the regions but it may distort them if the conditioning data are very dense (high number of borehole data).

Another limitation is the absence of a mechanism controlling the cross-correlation between successive surfaces. These structures are observed in sedimentary environments with laminations and cross-beds for example, (e.g., Miall, 1996; Siegenthaler & Huggenberger, 1993). But EROSim does not consider it for the moment, as we aim to keep the model simple and easy to parameterize. However, the principle of the surface-based method implemented in EROSim is flexible and this type of rule could be implemented in the future if needed. Additional complexity can also be added relatively easily by including non-stationarity when modeling the surfaces as shown in Figure 6. It is also possible to extend the parameterization of the facies attribution algorithm. More sophisticated rules involving transition probabilities between each facies, similar to what is done in TPROGs (Carle, 1999), could be accounted for. We could also consider the volume or shape of the region when estimating the probability of affecting a facies to a certain region. Finally, different statistical properties could have been used for onlap and erosive to distinguish these two different sedimentological processes. Indeed, it is expected that since they are the result of different processes, they should be relatively different in terms of the final surfaces produced. However, once again, we argue that the simplicity of the proposed model is probably sufficient for many applications and we leave this possible extensions to future works.

6. Conclusion

In this paper, we presented a new approach, EROSim, to model geological heterogeneity by simulating litho-facies models. The method is designed to represent sedimentary structures typically present in fluvio-glacial Quaternary deposits which are the most frequently used aquifers in Switzerland. EROSim offers a new perspective in the field of facies modeling by initially creating regions and subsequently populating them with facies. Moreover, it seamlessly integrates geological principles via erosion-deposition rules, introducing a significant degree of flexibility into its realizations and rendering it suitable for diverse sedimentological contexts. The litho-facies are assigned to the regions using a graph-based approach accounting for global proportions over the entire domain and for local proportions derived from adjacent regions. The conditioning algorithm employs inequality data derived from the borehole observations and the sedimentological rules.

The capacity of this model to represent different geometries and sedimentary patterns has been illustrated with several unconditional and conditional examples. Through these examples, we show the influence of the model parameters (e.g., α, ξ, etc.) on the resulting simulations. Furthermore, EROSim is applied to a real field site from a gravel quarry, where the spatial statistics of the sedimentological surfaces are inferred and used to parameterize the simulations. The resulting simulations show spatial patterns closely similar to those observed on the quarry walls. A numerical comparison of the proportions of the facies and the indicator variograms of the facies confirms this similarity. The results of advective transport confirm that EROSim is capable of reproducing the main structures that control flow better than the SIS simulation method.

The main advantages of EROSim are: its simplicity for the parameterization, its capacity to generate realistic 3D simulations from data acquired in 2D, its hierarchical structures, the possibility to condition the simulations by borehole data, and finally the availability of the code.

Further research is still needed to pursue the analyzis of the impact of the structures generated by EROSim on flow and solute transport and to further compare the performances of this model with other more sophisticated facies modeling techniques.

Appendix A

A1. Simulation Parameters

The various geostatistical parameters used in this study are listed below. We have the variograms used to generate the stochastic surfaces used in the EROSim simulations of the NS and EW walls of the Bümberg quarry (Tables A1 and A2). Table A3 shows the chosen EROSim parameters (number of surfaces, alpha parameter, frequency of erosive surfaces) for the different stratigraphic unit groups.

Table A1
Covariance Models Parameters (C: Contribution (Sill) and r: Range)

Quarry wall	Rank surfaces	r_{cub1} [m]	C_{cub1} (m^2)	r_{cub2} [m]	C_{cub2} (m^2)
NS	3 in unit 5	–	–	32	0.35
	3 in unit 4	15	0.27	30	0.39
	3 in unit 3	–	–	25	0.64
	3 in unit 2	–	–	35	1.06
	3 in unit 1	28	0.41	23	0.38
	4	–	–	90	0.26
	5	68	0.65	30	0.1
EW	3 in unit 5	–	–	44	0.44
	3 in unit 4	–	–	29	0.77
	3 in unit 3	–	–	35	0.55
	3 in unit 2	–	–	60	1.35
	3 in unit 1	70	0.51	45	0.29
	4	–	–	90	0.25
	5	25	0.12	60	0.15

Note. Subscripts *cub1* and *cub2* indicate two different cubic covariance models. Contributions that were lower than 0.01 were discarded.

Table A2
List of High-Order Surfaces With Their Rank and Mean Altitude Used for the Simulations

Quarry wall	Surface ID	Rank	Mean altitude [M]	Bottom of …	Top of …
NS	1	4	13.68	Unit 5	Unit 4
	2	4	10.99	Unit 4	Unit 3
	3	5	7.22	Unit 3	Unit 2
	4	4	4.43	Unit 2	Unit 1
EW	1	4	10.59	Unit 5	Unit 4
	2	4	8.23	Unit 4	Unit 3
	3	5	5.75	Unit 3	Unit 2
	4	4	3.90	Unit 2	Unit 1

Table A3
EROSim Parameters Used for the Simulation of the Quarry Walls

Quarry wall	Unit group	α	N	ξ	p_{global} (blue, brown, green, yellow)
NS	Unit 1	0.8	10	0.2	(0.5, 0, 0.1, 0.4)
	Unit 2	0.8	15	0.2	(0.32, 0, 0.31, 0.37)
	Unit 3	0.5	10	0.2	(0.20, 0, 0.35, 0.45)
	Unit 4	0.9	20	0.2	(0, 0, 0.50, 0.50)
	Unit 5	0.9	3	0.2	(0, 0, 0, 1)
EW	Unit 1	1	20	0.2	(0.10, 0.15, 0.10, 0.70)
	Unit 2	1	15	0.2	(0.08, 0, 0.12, 0.8)
	Unit 3	1	10	0.2	(0.05, 0, 0.22, 0.73)
	Unit 4	0.9	10	0.2	(0, 0.10, 0.50, 0.40)
	Unit 5	0.9	3	0.2	(0, 0, 0.10, 0.90)

Data Availability Statement

The code and data set used in this paper are accessible online at https://zenodo.org/records/12720720.

Acknowledgments
The authors wish to express their thanks to the sedimentological team of the University of Milano, Riccardo Bersezio, Chiara Zuffetti, Alessandro Comunian, Lucas Colombera and most particularly Ilaria Menga for her meticulous work on the geology of the Aar Valley, without which this work likely would nzot have been done. The authors wish also to thank Jeremy Bennett and Peter Bayer for their constructive suggestions when reviewing this paper.

References

Allard, D., Comunian, A., & Renard, P. (2012). Probability aggregation methods in geoscience. *Mathematical Geosciences*, *44*(5), 545–581. https://doi.org/10.1007/s11004-012-9396-3

Allen, J. (1978). Studies in fluviatile sedimentation: An exploratory quantitative model for the architecture of avulsion-controlled alluvial suites. *Sedimentary Geology*, *21*(2), 129–147. https://doi.org/10.1016/0037-0738(78)90002-7

Bakker, M., & Bot, B. (2024). The effective vertical anisotropy of layered aquifers. *Ground Water*, *63*(1), 68–75. https://doi.org/10.1111/gwat.13432

Bakker, M., Post, V., Langevin, C. D., Hughes, J. D., White, J. T., Starn, J., & Fienen, M. N. (2016). Scripting modflow model development using python and flopy. *Ground Water*, *54*(5), 733–739. https://doi.org/10.1111/gwat.12413

Bayer, P., Huggenberger, P., Renard, P., & Comunian, A. (2011). Three-dimensional high resolution fluvio-glacial aquifer analog: Part 1: Field study. *Journal of Hydrology*, *405*(1–2), 1–9. https://doi.org/10.1016/j.jhydrol.2011.03.038

Bennett, J. P., Haslauer, C. P., & Cirpka, O. A. (2017). The impact of sedimentary anisotropy on solute mixing in stacked scour-pool structures. *Water Resources Research*, *53*(4), 2813–2832. https://doi.org/10.1002/2016wr019665

Bennett, J. P., Haslauer, C. P., Ross, M., & Cirpka, O. A. (2019). An open, object-based framework for generating anisotropy in sedimentary subsurface models. *Ground Water*, *57*(3), 420–429. https://doi.org/10.1111/gwat.12803

Borghi, A., Renard, P., & Courrioux, G. (2015). Generation of 3d spatially variable anisotropy for groundwater flow simulations. *Ground Water*, *53*(6), 955–958. https://doi.org/10.1111/gwat.12295

Bridge, J. S., & Leeder, M. R. (1979). A simulation model of alluvial stratigraphy. *Sedimentology*, *26*(5), 617–644. https://doi.org/10.1111/j.1365-3091.1979.tb00935.x

Carle, S. F. (1999). *T-progs: Transition probability geostatistical software, version 2.1*. Department of Land, Air and Water Resources, University of California.

Chiles, J.-P., & Delfiner, P. (2012). *Geostatistics: Modeling spatial uncertainty* (Vol. 713). John Wiley & Sons. https://doi.org/10.1002/9781118136188

Chiogna, G., Cirpka, O. A., Rolle, M., & Bellin, A. (2015). Helical flow in three-dimensional nonstationary anisotropic heterogeneous porous media. *Water Resources Research*, *51*(1), 261–280. https://doi.org/10.1002/2014wr015330

Comunian, A., Renard, P., Straubhaar, J., & Bayer, P. (2011). Three-dimensional high resolution fluvio-glacial aquifer analog–Part 2: Geostatistical modeling. *Journal of Hydrology*, *405*(1–2), 10–23. https://doi.org/10.1016/j.jhydrol.2011.03.037

Dagan, G. (1989). *Flow and transport in porous formations*. Springer Science & Business Media.

de Marsily, G., Delay, F., Gonçalvès, J., Renard, P., Teles, V., & Violette, S. (2005). Dealing with spatial heterogeneity. *Hydrogeology Journal*, *13*(1), 161–183. https://doi.org/10.1007/s10040-004-0432-3

Freulon, X., & de Fouquet, C. (1993). Conditioning a Gaussian model with inequalities. *Geostatistics Tróia'92*, *1*, 201–212. https://doi.org/10.1007/978-94-011-1739-5_17

Geng, X., Michael, H. A., Boufadel, M. C., Molz, F. J., Gerges, F., & Lee, K. (2020). Heterogeneity affects intertidal flow topology in coastal beach aquifers. *Geophysical Research Letters*, *47*(17), e2020GL089612. https://doi.org/10.1029/2020gl089612

Haldorsen, H. H., & Lake, L. W. (1984). A new approach to shale management in field-scale models. *Society of Petroleum Engineers Journal*, *24*(04), 447–457. https://doi.org/10.2118/10976-pa

Heinz, J., Kleineidam, S., Teutsch, G., & Aigner, T. (2003). Heterogeneity patterns of quaternary glaciofluvial gravel bodies (SW-Germany): Application to hydrogeology. *Sedimentary Geology*, *158*(1–2), 1–23. https://doi.org/10.1016/s0037-0738(02)00239-7

Huysmans, M., & Dassargues, A. (2012). Modeling the effect of clay drapes on pumping test response in a cross-bedded aquifer using multiple-point geostatistics. *Journal of Hydrology*, *450*, 159–167. https://doi.org/10.1016/j.jhydrol.2012.05.014

Jo, H., Santos, J. E., & Pyrcz, M. J. (2020). Conditioning well data to rule-based lobe model by machine learning with a generative adversarial network. *Energy Exploration & Exploitation*, *38*(6), 2558–2578. https://doi.org/10.1177/0144598720937524

Journel, A. G., & Alabert, F. G. (1990). New method for reservoir mapping. *Journal of Petroleum Technology*, *42*(02), 212–218. https://doi.org/10.2118/18324-pa

Juda, P., Renard, P., & Straubhaar, J. (2020). A framework for the cross-validation of categorical geostatistical simulations. *Earth and Space Science*, *7*(8), e2020EA001152. https://doi.org/10.1029/2020ea001152

Kitanidis, P. K. (2015). Persistent questions of heterogeneity, uncertainty, and scale in subsurface flow and transport. *Water Resources Research*, *51*(8), 5888–5904. https://doi.org/10.1002/2015wr017639

Koltermann, C. E., & Gorelick, S. M. (1996). Heterogeneity in sedimentary deposits: A review of structure-imitating, process-imitating, and descriptive approaches. *Water Resources Research*, *32*(9), 2617–2658. https://doi.org/10.1029/96wr00025

Koneshloo, M., Kreyns, P., & Michael, H. A. (2018). Combining process-based and surface-based models to simulate subsurface heterogeneity in volcanic aquifers. *Stochastic Environmental Research and Risk Assessment*, *32*(9), 2565–2583. https://doi.org/10.1007/s00477-018-1511-7

Langevin, C. D., Hughes, J. D., Banta, E. R., Niswonger, R. G., Panday, S., & Provost, A. M. (2017). *Documentation for the modflow 6 groundwater flow model* (Tech. Rep.). US Geological Survey.

Mariethoz, G., Renard, P., & Straubhaar, J. (2010). The Direct Sampling method to perform multiple-point geostatistical simulations. *Water Resources Research*, *46*(11). https://doi.org/10.1029/2008WR007621

Menga, I. (2021). *Analysis of late pleistocene aquifer analogues to characterize heterogeneity of the post glacial aquifers of the Aare valley (Switzerland)* (Unpublished master's thesis). Universita' degli studi di Milano, facoltà di Scienze e Tecnologie, Via Luigi Mangiagalli.

Miall, A. (1996). *The geology of fluvial deposits. Sedimentary facies, basin analysis, and petroleum geology*. Springer.

Neuman, S. P., Riva, M., & Guadagnini, A. (2008). On the geostatistical characterization of hierarchical media. *Water Resources Research*, *44*(2). https://doi.org/10.1029/2007wr006228

Neven, A., Christiansen, A. V., & Renard, P. (2022). Automatic stochastic 3D clay fraction model from tTEM survey and borehole data. *Scientific Reports*, *12*(1), 17112. https://doi.org/10.1038/s41598-022-21555-z

Neven, A., & Renard, P. (2023). A novel methodology for the stochastic integration of geophysical and hydrogeological data in geologically consistent models. *Water Resources Research*, *59*(7), e2023WR034992. https://doi.org/10.1029/2023wr034992

Neven, A., Schorpp, L., & Renard, P. (2022). Stochastic multi-fidelity joint hydrogeophysical inversion of consistent geological models. *Frontiers in Water*, *4*, 989440. https://doi.org/10.3389/frwa.2022.989440

Pirmez, C., Beaubouef, R., Friedmann, S., & Mohrig, D. (2000). Equilibrium profile and baselevel in submarine channels: Examples from late pleistocene systems and implications for the architecture of deepwater reservoirs. In *Deep-Water Reservoirs of the World: 20th Annual* (pp. 782–805). https://doi.org/10.5724/gcs.00.15.0782

Pirot, G., Straubhaar, J., & Renard, P. (2015). A pseudo genetic model of coarse braided-river deposits. *Water Resources Research*, *51*(12), 9595–9611. https://doi.org/10.1002/2015wr017078

Pollock, D. W. (2016). *User guide for modpath version 7—A particle-tracking model for modflow* (Tech. Rep.). US Geological Survey.

Pyrcz, M. J., Catuneanu, O., & Deutsch, C. V. (2005). Stochastic surface-based modeling of turbidite lobes. *AAPG Bulletin*, *89*(2), 177–191. https://doi.org/10.1306/09220403112

Pyrcz, M. J., & Deutsch, C. V. (2014). *Geostatistical reservoir modeling*. Oxford University Press.

Pyrcz, M. J., Sech, R. P., Covault, J. A., Willis, B. J., Sylvester, Z., Sun, T., & Garner, D. (2015). Stratigraphic rule-based reservoir modeling. *Bulletin of Canadian Petroleum Geology*, *63*(4), 287–303. https://doi.org/10.2113/gscpgbull.63.4.287

Ramanathan, R., Guin, A., Ritzi Jr, R. W., Dominic, D. F., Freedman, V. L., Scheibe, T. D., & Lunt, I. A. (2010). Simulating the heterogeneity in braided channel belt deposits: 1. A geometric-based methodology and code. *Water Resources Research*, *46*(4). https://doi.org/10.1029/2009wr008111

Renard, P., & Ababou, R. (2022). Equivalent permeability tensor of heterogeneous media: Upscaling methods and criteria (review and analyses). *Geosciences*, *12*(7), 269. https://doi.org/10.3390/geosciences12070269

Ritzi, R. W., Dai, Z., Dominic, D. F., & Rubin, Y. N. (2004). Spatial correlation of permeability in cross-stratified sediment with hierarchical architecture. *Water Resources Research*, *40*(3). https://doi.org/10.1029/2003wr002420

Rongier, G., Collon, P., & Renard, P. (2017). Stochastic simulation of channelized sedimentary bodies using a constrained l-system. *Computers & Geosciences*, *105*, 158–168. https://doi.org/10.1016/j.cageo.2017.05.006

Rubin, Y. (2003). *Applied stochastic hydrogeology*. Oxford University Press.

Scheibe, T. D., & Freyberg, D. L. (1995). Use of sedimentological information for geometric simulation of natural porous media structure. *Water Resources Research*, *31*(12), 3259–3270. https://doi.org/10.1029/95wr02570

Schlüchter, C. (1973). Die Münsingenschotter, ein letzteiszeitlicher Schotterkörper im Aaretal südlich von Bern. Bulletin der Vereinigung Schweiz. *Petroleum-Geologen und-Ingenieure*, *39*(0096), 69–78.

Schlüchter, C., Akçar, N., & Ivy-Ochs, S. (2021). The quaternary period in Switzerland. In *Landscapes and landforms of Switzerland* (pp. 47–69).

Schorpp, L., Straubhaar, J., & Renard, P. (2022). Automated hierarchical 3d modeling of quaternary aquifers: The archpy approach. *Frontiers in Earth Science*, *10*, 884075. https://doi.org/10.3389/feart.2022.884075

Shannon, C. E. (1948). A mathematical theory of communication. *The Bell System Technical Journal*, *27*(3), 379–423. https://doi.org/10.1002/j.1538-7305.1948.tb01338.x

Siegenthaler, C., & Huggenberger, P. (1993). Pleistocene rhine gravel: Deposits of a braided river system with dominant pool preservation. *Geological Society, London, Special Publications*, *75*(1), 147–162. https://doi.org/10.1144/gsl.sp.1993.075.01.09

Solomina, O. N., Bradley, R. S., Hodgson, D. A., Ivy-Ochs, S., Jomelli, V., Mackintosh, A. N., et al. (2015). Holocene glacier fluctuations. *Quaternary Science Reviews*, *111*, 9–34. https://doi.org/10.1016/j.quascirev.2014.11.018

Soltanian, M. R., Behzadi, F., & de Barros, F. P. (2020). Dilution enhancement in hierarchical and multiscale heterogeneous sediments. *Journal of Hydrology*, *587*, 125025. https://doi.org/10.1016/j.jhydrol.2020.125025

Strebelle, S. (2002). Conditional simulation of complex geological structures using multiple-point statistics. *Mathematical Geology*, *34*, 1–21. https://doi.org/10.1023/a:1014009426274

Titus, Z., Heaney, C., Jacquemyn, C., Salinas, P., Jackson, M., & Pain, C. (2021). Conditioning surface-based geological models to well data using artificial neural networks. *Computational Geosciences*, *26*(4), 1–24. https://doi.org/10.1007/s10596-021-10088-5

Wallace, C. D., Tonina, D., McGarr, J. T., de Barros, F. P., & Soltanian, M. R. (2021). Spatiotemporal dynamics of nitrous oxide emission hotspots in heterogeneous riparian sediments. *Water Resources Research*, *57*(12), e2021WR030496. https://doi.org/10.1029/2021wr030496

Webb, E. K. (1994). Simulating the three-dimensional distribution of sediment units in braided-stream deposits. *Journal of Sedimentary Research*, *64*(2b), 219–231. https://doi.org/10.1306/d4267f96-2b26-11d7-8648000102c1865d

Wentworth, C. K. (1922). A scale of grade and class terms for clastic sediments. *The Journal of Geology*, *30*(5), 377–392. https://doi.org/10.1086/622910

Xie, Y., Cullick, A. S., & Deutsch, C. V. (2001). Surface-geometry and trend modeling for integration of stratigraphic data in reservoir models. In *Spe western regional meeting*.

Xie, Y., Deutsch, C. V., & Cullick, A. (1999). A short note on surface-based modelling for integration of stratigraphic data in geostatistical reservoir models. In *CCG Annual Report One*. University of Alberta.

Zech, A., Attinger, S., Bellin, A., Cvetkovic, V., Dagan, G., Dentz, M., et al. (2021). A comparison of six transport models of the made-1 experiment implemented with different types of hydraulic data. *Water Resources Research*, *57*(5), e2020WR028672. https://doi.org/10.1029/2020wr028672

Zuffetti, C., Comunian, A., Bersezio, R., & Renard, P. (2020). A new perspective to model subsurface stratigraphy in alluvial hydrogeological basins, introducing geological hierarchy and relative chronology. *Computers & Geosciences*, *140*, 104506. https://doi.org/10.1016/j.cageo.2020.104506